PPARα activation is essential for HCV core protein–induced hepatic steatosis and hepatocellular carcinoma in mice

Naoki Tanaka,[1,2] Kyoji Moriya,[3] Kendo Kiyosawa,[2] Kazuhiko Koike,[3] Frank J. Gonzalez,[4] and Toshifumi Aoyama[1]

[1]Department of Metabolic Regulation, Institute on Aging and Adaptation, Shinshu University Graduate School of Medicine, Matsumoto, Nagano, Japan.
[2]Division of Gastroenterology, Department of Internal Medicine, Shinshu University School of Medicine, Matsumoto, Nagano, Japan.
[3]Department of Infectious Diseases, Internal Medicine, Graduate School of Medicine, University of Tokyo, Tokyo, Japan.
[4]Laboratory of Metabolism, National Cancer Institute, NIH, Bethesda, Maryland, USA.

Transgenic mice expressing HCV core protein develop hepatic steatosis and hepatocellular carcinoma (HCC), but the mechanism underlying this process remains unclear. Because PPARα is a central regulator of triglyceride homeostasis and mediates hepatocarcinogenesis in rodents, we determined whether PPARα contributes to HCV core protein–induced diseases. We generated PPARα-homozygous, -heterozygous, and -null mice with liver-specific transgenic expression of the core protein gene (*Ppara*$^{+/+}$:HCVcpTg, *Ppara*$^{+/-}$:HCVcpTg, and *Ppara*$^{-/-}$:HCVcpTg mice. Severe steatosis was unexpectedly observed only in *Ppara*$^{+/+}$:HCVcpTg mice, which resulted from enhanced fatty acid uptake and decreased mitochondrial β-oxidation due to breakdown of mitochondrial outer membranes. Interestingly, HCC developed in approximately 35% of 24-month-old *Ppara*$^{+/+}$:HCVcpTg mice, but tumors were not observed in the other genotypes. These phenomena were found to be closely associated with sustained PPARα activation. In *Ppara*$^{+/-}$:HCVcpTg mice, PPARα activation and the related changes did not occur despite the presence of a functional *Ppara* allele. However, long-term treatment of these mice with clofibrate, a PPARα activator, induced HCC with mitochondrial abnormalities and hepatic steatosis. Thus, our results indicate that persistent activation of PPARα is essential for the pathogenesis of hepatic steatosis and HCC induced by HCV infection.

Introduction

HCV is one of the major causes of chronic hepatitis, whereas patients with persistent HCV infection have a high incidence of hepatocellular carcinoma (HCC) (1, 2). Occurrence of HCC associated with chronic HCV infection has increased over the past 2 decades (3–5), and chronic HCV infection is recognized as a serious debilitating disease. However, the mechanism in which chronic HCV infection mediates hepatocarcinogenesis remains unclear.

HCV core protein was shown to have oncogenic potential (6). To examine how HCV core protein participates in HCV-related hepatocarcinogenesis, transgenic mouse lines were established in which HCV core protein is expressed constitutively in liver at cellular levels similar to those found in chronic HCV-infected patients (7). These mice exhibited hepatic steatosis (7) and insulin resistance (8) as early as 3 months of age; on further aging, these symptoms worsened and hepatic adenomas developed in approximately 30% of mice between 16 and 18 months of age (9). Finally, HCC was found within hepatic adenomas in a classic "nodule-in-nodule" pathology (9). Interestingly, no hepatic inflammation or fibrosis was found in these mice throughout the course of HCC development (9), which suggested that the HCV core protein itself induces hepatic steatosis and HCC independently of hepatitis.

Several studies support the contention that hepatic steatosis promotes the development of HCC (10). Epidemiologic data have identified hepatic steatosis as a major accelerating factor of hepatocarcinogenesis in chronic HCV-infected patients (11). Moreover, increases in ROS production that can cause oxidative DNA damage, mitochondrial abnormalities, and accelerated hepatocyte proliferation were observed in the steatotic livers (12–14). Thus, an intriguing possibility has emerged that alteration of fatty acid metabolism in hepatocytes may be central to the pathogenesis of HCC induced by HCV core protein.

PPARs are ligand-activated nuclear receptors belonging to the steroid/thyroid hormone receptor superfamily; 3 isoforms designated as α, β/δ, and γ exist, all of which are involved in lipid homeostasis (15). PPARα regulates constitutive transcription of genes encoding fatty acid–metabolizing enzymes (16) and is associated with the maintenance of fatty acid transport and metabolism, primarily in liver, kidney, and heart. Administration of PPARα agonists, such as the widely prescribed fibrate drugs clofibrate, gemfibrozil, and fenofibrate, ameliorate hyperlipidemia in humans (17) and hepatic steatosis in mice (18).

On the other hand, long-term administration of PPARα ligands to rodents causes accelerated hepatocyte proliferation, increased ROS generation, and development of HCC (19, 20). Disruption of the PPARα gene was shown to prevent the development of HCC caused by long-term exposure to PPARα activators (21). Interestingly, accumulation of fatty acids/triglycerides in hepatocytes

Nonstandard abbreviations used: ACC, acetyl-CoA carboxylase; AOX, acyl-CoA oxidase; CDK, cyclin-dependent kinase; CYP4A1, cytochrome P450 4A1; FAS, fatty acid synthase; FAT, fatty acid translocase; FATP, fatty acid transport protein; HCC, hepatocellular carcinoma; HCVcpTg, HCV core protein–expressing transgenic; L-FABP, liver fatty acid-binding protein; MCAD, medium-chain acyl-CoA dehydrogenase; MTP, microsomal transfer protein; 8-OHdG, 8-hydroxy-2′-deoxyguanosine; PCNA, proliferating cell nuclear antigen; RXRα, retinoid X receptor α.

Conflict of interest: The authors have declared that no conflict of interest exists.

Citation for this article: *J. Clin. Invest.* **118**:683–694 (2008). doi:10.1172/JCI33594.

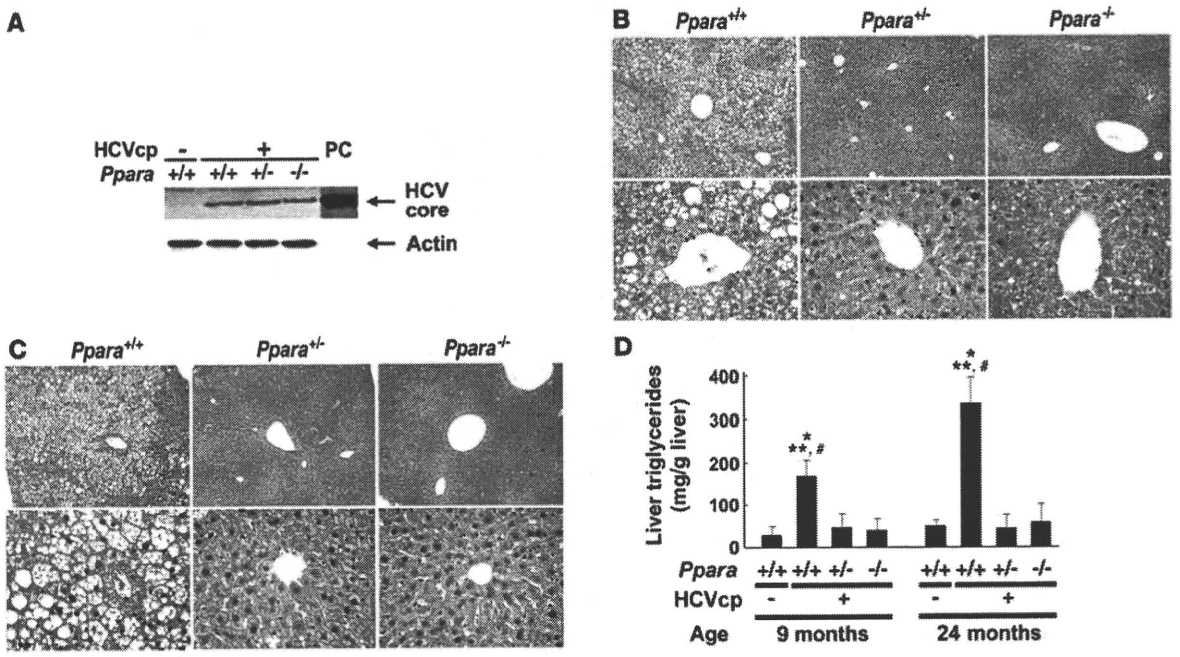

Figure 1

Phenotype changes in transgenic mouse liver. (**A**) Immunoblot analysis of HCV core protein expression in livers of 9-month-old mice. Because no significant individual differences in the same mouse group were found in the preliminary experiments, 10 mg of liver prepared from each mouse ($n = 6$/group) was mixed and homogenized. Whole-liver lysate (50 μg protein) was loaded in each well. The band of actin was used as the loading control. Results are representative of 4 independent experiments. PC, lysate prepared from COS-1 cells overexpressing HCV core protein as a positive control. (**B**) Histological appearance of hematoxylin- and eosin-stained liver sections from 9-month-old HCVcpTg mice. Upper and lower rows show a lower (×40) and higher (×400) magnification, respectively. Microvesicular and macrovesicular steatosis was found only in *Ppara*$^{+/+}$:HCVcpTg mice. No inflammation or hepatocyte degeneration was evident in any of the genotypes. (**C**) Histological appearance of hematoxylin- and eosin-stained liver sections from 24-month-old HCVcpTg mice. Upper and lower rows show a lower (×40) and higher (×400) magnification, respectively. Hepatic steatosis was marked in *Ppara*$^{+/+}$:HCVcpTg mice, but not in other mice. Hepatic inflammation, fibrosis, and hepatocyte degeneration were not observed. In *Ppara*$^{+/-}$:HCVcpTg and *Ppara*$^{-/-}$:HCVcpTg mice, dysplastic hepatocytes and precancerous lesions were not detected throughout the entire liver. (**D**) Content of liver triglycerides. Results are expressed as the mean ± SD ($n = 6$/group) and compared between genotypes at the same age. $^{*}P < 0.05$ compared with *Ppara*$^{+/+}$ nontransgenic mice; $^{**}P < 0.05$ compared with *Ppara*$^{+/-}$:HCVcpTg mice; $^{\#}P < 0.05$ compared with *Ppara*$^{-/-}$:HCVcpTg mice.

could lead to continuous PPARα activation because of the presence of fatty acid metabolites that serve as natural PPARα ligands. For example, mice lacking expression of the peroxisomal acyl-CoA oxidase (AOX) gene showed massive accumulation of very-long-chain fatty acids in hepatocytes, severe microvesicular steatosis, chronic PPARα activation, and development of hepatic adenoma and HCC by 15 months of age (22). These results suggest a strong contribution of activated PPARα to liver tumorigenesis.

On the basis of several lines of evidence, we hypothesized that PPARα might contribute to hepatocarcinogenesis in HCV core protein-expressing transgenic (HCVcpTg) mice. To explore this possibility, PPARα-homozygous (*Ppara*$^{+/+}$), PPARα-heterozygous (*Ppara*$^{+/-}$), and PPARα-null (*Ppara*$^{-/-}$) mice bearing the HCV core protein gene, designated *Ppara*$^{+/+}$:HCVcpTg, *Ppara*$^{+/-}$:HCVcpTg, and *Ppara*$^{-/-}$:HCVcpTg mice, were generated, and phenotypic changes were examined. Surprisingly, we found that severe hepatic steatosis and HCC induced by HCV core protein developed only in *Ppara*$^{+/+}$ mice, which were related to persistent PPARα activation.

Results

Expression of HCV core protein in transgenic mice. *Ppara*$^{-/-}$:HCVcpTg and *Ppara*$^{+/-}$:HCVcpTg mice appeared healthy, and body weight in both genotypes was similar to that of *Ppara*$^{+/+}$:HCVcpTg and *Ppara*$^{+/+}$ mice without the transgene. When hepatic expression of HCV core protein in 9-month-old transgenic mice was examined by immunoblot analysis, it was similar among *Ppara*$^{+/+}$:HCVcpTg, *Ppara*$^{+/-}$:HCVcpTg, and *Ppara*$^{-/-}$:HCVcpTg mice (Figure 1A) and was also similar to expression in HCVcpTg mice reported previously (7, 9). Age and sex had only a minor influence on the hepatic expression of HCV core protein.

Requirement of homozygous PPARα for the development of hepatic steatosis in transgenic mice. Livers of 9-month-old male HCVcpTg mice with or without the *Ppara* allele were examined. Those of *Ppara*$^{+/+}$:HCVcpTg mice were soft, slightly enlarged, and light in color and histologically showed macrovesicular and microvesicular steatosis with no apparent inflammation or hepatocyte necrosis (Figure 1B), in agreement with previous reports (7, 9). Biochemical analysis of liver extracts showed marked hepatic accumulation of triglycerides (Figure 1D). In contrast, livers of 9-month-old *Ppara*$^{+/-}$:HCVcpTg and *Ppara*$^{-/-}$:HCVcpTg mice showed neither histological abnormalities nor accumulation of triglycerides (Figure 1, B and D). Hepatic levels of free fatty acids in *Ppara*$^{+/+}$:HCVcpTg mice were approximately 3 times those in *Ppara*$^{+/-}$:HCVcpTg and *Ppara*$^{-/-}$:HCVcpTg mice or *Ppara*$^{+/+}$ mice not expressing the HCV core protein.

In 24-month-old *Ppara*$^{+/+}$:HCVcpTg mice, hepatic steatosis was found (Figure 1C), and the hepatic levels of triglycerides were further increased (Figure 1D). Apparent inflammation, hepatocyte

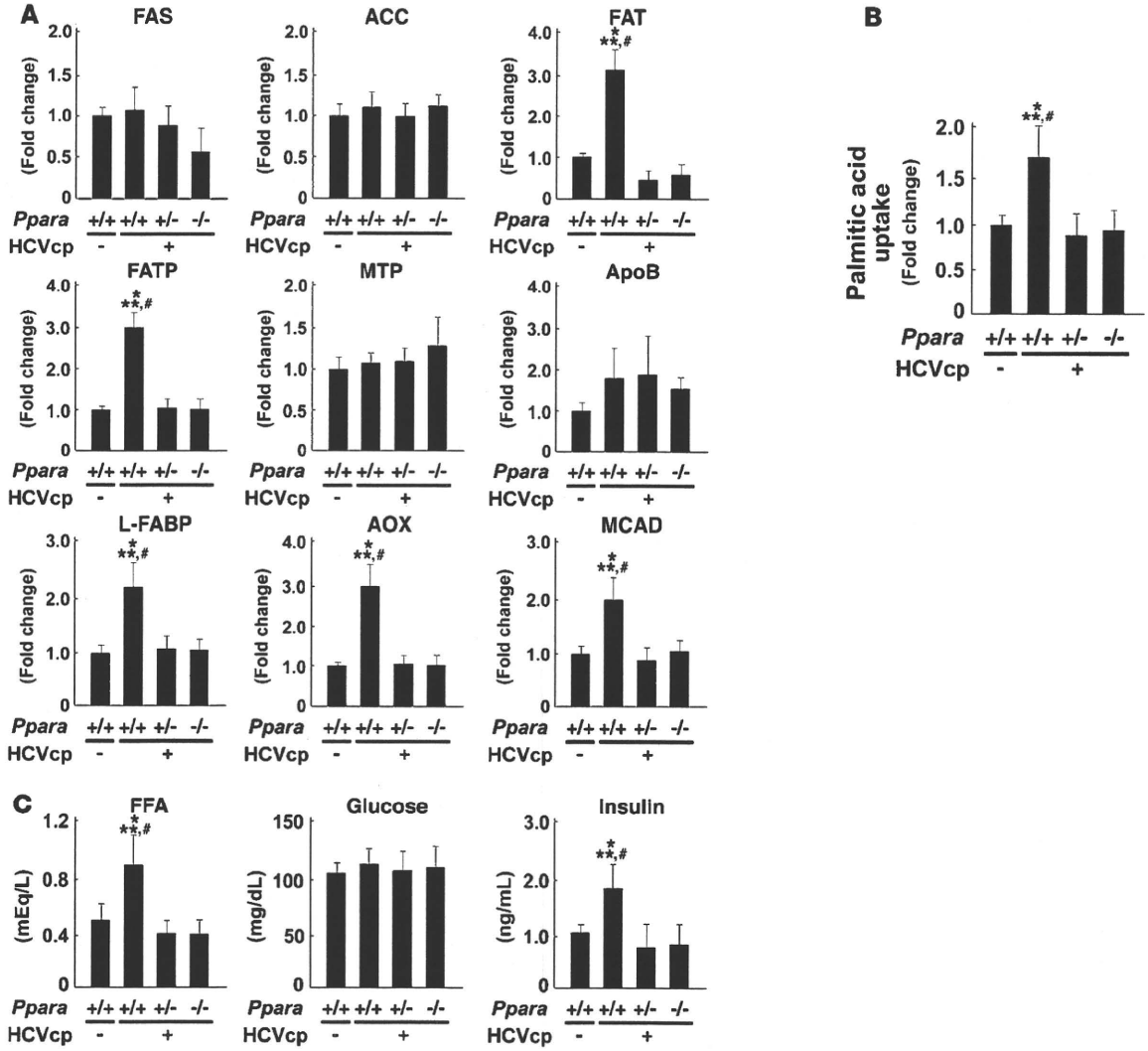

Figure 2

Analyses of factors associated with hepatic fatty acid and triglyceride metabolism. (**A**) Expression of genes associated with fatty acid and triglyceride metabolism in 9-month-old mouse livers. Total RNA was extracted from each mouse liver, and mRNA levels were determined by RT-PCR. mRNA levels were normalized by those of GAPDH and subsequently normalized by those in *Ppara*$^{+/+}$ nontransgenic mice. Results are expressed as the mean ± SD (n = 6/group). *P < 0.05 compared with *Ppara*$^{+/+}$ nontransgenic mice; **P < 0.05 compared with *Ppara*$^{+/-}$:HCVcpTg mice; #P < 0.05 compared with *Ppara*$^{-/-}$:HCVcpTg mice. (**B**) Uptake of fatty acids in 9-month-old mouse livers. Liver slices obtained from 3 mice in each group were incubated in medium containing 0.8 mM [1-^{14}C]palmitic acid for 7 h. Fatty acid uptake ability was estimated by the sum of palmitic acid converted to CO_2 and ketone bodies with that incorporated into total cellular lipids after incubation. The experiment was repeated 3 times. Results were normalized by those of *Ppara*$^{+/+}$ nontransgenic mice and expressed as the mean ± SD. (**C**) Plasma concentrations of free fatty acids, glucose, and insulin. After an overnight fast, blood was obtained from each mouse and the above variables were determined. Results are expressed as the mean ± SD (n = 6/group).

degeneration and necrosis, and fibrosis were not detected. On the other hand, *Ppara*$^{+/-}$:HCVcpTg and *Ppara*$^{-/-}$:HCVcpTg mice showed no steatosis (Figure 1, C and D). These results indicate that hepatic steatosis develops in *Ppara*$^{+/+}$:HCVcpTg mice, but not in *Ppara*$^{+/-}$:HCVcpTg and *Ppara*$^{-/-}$:HCVcpTg mice.

Hepatic fatty acid and triglyceride metabolism in transgenic mice. To investigate the mechanism responsible for the development of severe steatosis in *Ppara*$^{+/+}$:HCVcpTg mice, the expression of genes associated with fatty acid and triglyceride metabolism in the livers of 9-month-old mice was analyzed using the quantitative RT-PCR method. As shown in Figure 2A, the mRNA levels of genes related to de novo lipogenesis (fatty acid synthase [FAS] and acetyl-CoA carboxylase [ACC]) and secretion of VLDL (microsomal transfer protein [MTP] and apoB) were constant in all groups. The mRNA levels of fatty acid translocase (FAT) and fatty acid transport protein (FATP), which are associated with the uptake of fatty acids into hepatocytes, were significantly increased only in *Ppara*$^{+/+}$:HCVcpTg mice, but the mRNA levels of hepatic triglyceride lipase, another contributor to fatty acid uptake, remained unchanged (data not shown). The mRNA levels of liver fatty acid binding protein (L-FABP) were also elevated only in *Ppara*$^{+/+}$:HCVcpTg mice. Surprisingly, the mRNA levels of AOX and medium-chain acyl-CoA

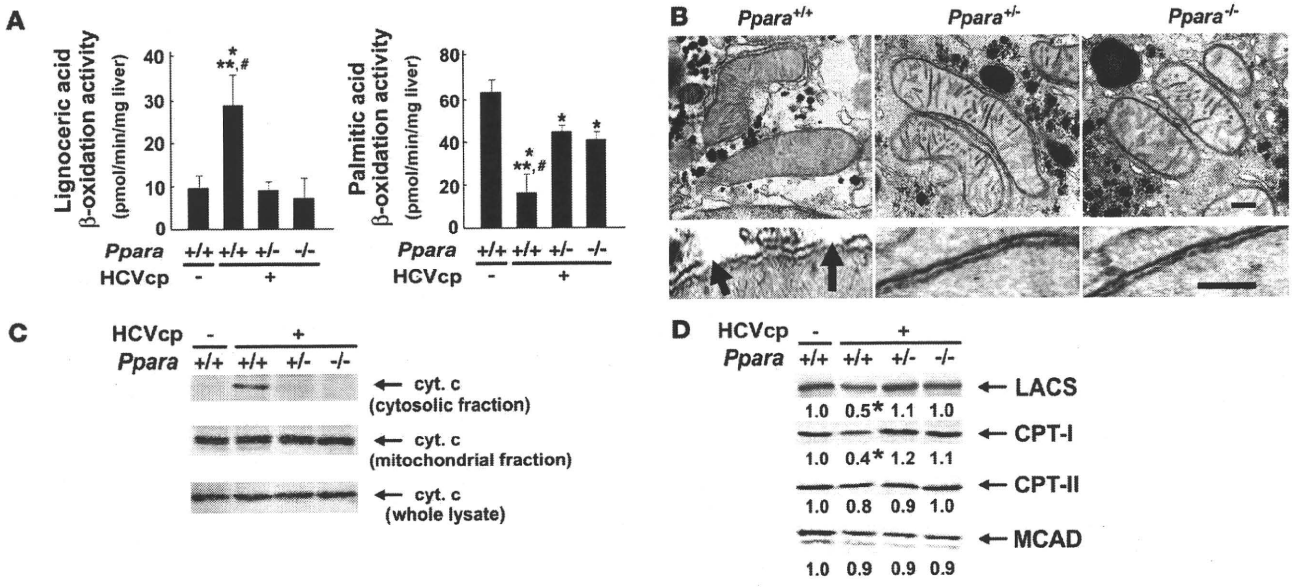

Figure 3

Analyses of mitochondrial abnormalities. (**A**) Lignoceric and palmitic acid β-oxidation activities in 9-month-old mice. Results are expressed as the mean ± SD (n = 6/group). *P < 0.05 compared with *Ppara*$^{+/+}$ nontransgenic mice; **P < 0.05 compared with *Ppara*$^{+/-}$:HCVcpTg mice; $^{\#}P$ < 0.05 compared with *Ppara*$^{-/-}$:HCVcpTg mice. (**B**) Electron microscopic features of hepatic mitochondria of 9-month-old HCVcpTg mice. Upper and lower rows show a lower and higher magnification, respectively. In *Ppara*$^{+/+}$:HCVcpTg mice, some mitochondria showing discontinuance of outer membranes (arrows) and amorphous inner structures were observed. In *Ppara*$^{+/-}$:HCVcpTg and *Ppara*$^{-/-}$:HCVcpTg mice, mitochondria appeared normal; the scale bars represent 200 nm (top) and 30 nm (bottom), respectively. (**C**) Immunoblot analysis of cytochrome *c* in 9-month-old mice. Whole-liver lysate, mitochondrial fraction, or cytosolic fraction (50 μg protein) was loaded in each well. Results are representative of 4 independent experiments. (**D**) Immunoblot analysis of representative mitochondrial β-oxidation enzymes using a mitochondrial fraction prepared from 9-month-old mouse livers. The mitochondrial fraction (20 μg protein) was loaded in each well. Results are representative of 4 independent experiments. The band intensity was quantified densitometrically and normalized by that in *Ppara*$^{+/+}$ nontransgenic mouse. The mean value of the fold changes is shown under the representative band. LACS, long-chain acyl-CoA synthase; CPT, carnitine palmitoyl-CoA transferase.

dehydrogenase (MCAD), a rate-limiting enzymes in the peroxisomal and mitochondrial β-oxidation pathways, respectively, were significantly increased in *Ppara*$^{+/+}$:HCVcpTg mice. When fatty acid uptake ability was measured in fresh liver slices, it was significantly enhanced only in *Ppara*$^{+/+}$:HCVcpTg mice (Figure 2B). Additionally, plasma free fatty acid levels were higher in these mice than in mice in the other groups. Although there were no differences in fasting plasma glucose levels between the groups, hyperinsulinemia was observed only in *Ppara*$^{+/+}$:HCVcpTg mice (Figure 2C), in agreement with the previous observation that significant insulin resistance developed in these mice (8). Similar results were obtained from 24-month-old mice (data not shown). These results combined show that the increased plasma fatty acid levels, which were likely due to enhanced peripheral fatty acid release caused by insulin resistance, and the increase in fatty acid uptake ability are consistent with steatogenesis in *Ppara*$^{+/+}$:HCVcpTg mice.

Decreased mitochondrial β-oxidation in transgenic mice. Although the transcriptional activities of major β-oxidation enzymes were markedly increased, *Ppara*$^{+/+}$:HCVcpTg mice had severe steatosis. To explore this discrepant result, peroxisomal and mitochondrial β-oxidation activities were measured using lignoceric and palmitic acids as substrates, respectively. The lignoceric acid–degrading capacity was increased only in *Ppara*$^{+/+}$:HCVcpTg mice, where it corresponded to an increase in AOX expression. However, the capacity for palmitic acid degradation, which occurs particularly in mitochondria, was significantly lower in *Ppara*$^{+/+}$:HCVcpTg mice than in *Ppara*$^{+/-}$:HCVcpTg and *Ppara*$^{-/-}$:HCVcpTg mice (Figure 3A). Thus, decreased mitochondrial β-oxidation ability was considered to be another important mechanism for the development of steatosis induced by the core protein.

We further evaluated mitochondrial abnormalities. In electron microscopic examination, discontinuous outer membranes (Figure 3B, arrows) and lack of an internal structure were observed in some mitochondria of *Ppara*$^{+/+}$:HCVcpTg mouse livers, in agreement with the previous report (9). However, these abnormalities were not seen in *Ppara*$^{+/-}$:HCVcpTg and *Ppara*$^{-/-}$:HCVcpTg mice (Figure 3B). Immunoblot analysis showed that cytochrome *c*, which is usually localized in the mitochondrial intermembrane space, was present in the cytosolic fractions of *Ppara*$^{+/+}$:HCVcpTg mice (Figure 3C). Moreover, immunoblot analysis using mitochondrial fractions showed that the expression levels of long-chain acyl-CoA synthase and carnitine palmitoyl-CoA transferase-I, which are enzymes indispensable to the initial step of mitochondrial β-oxidation and are localized mainly in mitochondrial outer membranes, were significantly decreased only in *Ppara*$^{+/+}$:HCVcpTg mice (Figure 3D).

Overall, these results suggest that homozygous PPARα is essential to the pathogenesis of hepatic steatosis induced by the HCV core protein, which results from a decrease in mitochondrial fatty acid degradation capacity caused by the breakdown of mitochondrial outer membranes and a disproportionate increase in the uptake of fatty acids. Interestingly, steatosis and the related changes did not occur in *Ppara*$^{+/-}$ and *Ppara*$^{-/-}$ mice expressing the HCV core protein, which suggested that these changes were not caused by the core protein itself.

Table 1
Incidence of HCC in 24-month-old mice

HCV core protein	*Ppara*	Mice (*n*)	Mice with HCC (*n*)	Incidence (%)
–	+/+	20	0	0
–	+/–	18	0	0
–	–/–	20	0	0
+	+/+	17	6	35.3[A]
+	+/–	16	0	0
+	–/–	14	0	0

Mice were killed at 24 months of age for analysis. HCC was diagnosed according to histological findings. [A]$P < 0.05$ compared with *Ppara*$^{+/+}$ nontransgenic mice, $P < 0.05$ compared with *Ppara*$^{+/-}$:HCVcpTg mice, $P < 0.05$ compared with *Ppara*$^{-/-}$:HCVcpTg mice.

Requirement of homozygous PPARα for hepatic tumor development in transgenic mice. At 9 months of age, hepatic nodules were not observed at all in transgenic mice, whereas, at 24 months, approximately 35% of *Ppara*$^{+/+}$:HCVcpTg mice had macroscopically evident hepatic nodules (Table 1). Microscopically, these nodules had the appearance of well-differentiated HCC with trabecular features, which was consistent with the previous report (9). Surprisingly, *Ppara*$^{+/-}$:HCVcpTg and *Ppara*$^{-/-}$:HCVcpTg mice of the same ages developed no evidence of hepatic tumors, despite the expression of HCV core protein at similar levels to those found in *Ppara*$^{+/+}$:HCVcpTg mice (Table 1). Microscopic examination showed that there were no dysplastic cells or precancerous lesions throughout the livers in *Ppara*$^{+/-}$:HCVcpTg and *Ppara*$^{-/-}$:HCVcpTg mice (Figure 1C). These results provide strong evidence that homozygous PPARα is essential for hepatic tumorigenesis induced by HCV core protein.

Increased hepatocyte proliferation only in Ppara$^{+/+}$*:HCVcpTg mice.* Because sustained acceleration of hepatocyte proliferation relative to apoptosis may promote the development of HCC, these opposing processes were quantified in the livers of 24-month-old mice. Both the liver-to-body weight ratio and the number of hepatocytes expressing proliferating cell nuclear antigen (PCNA) were increased only in *Ppara*$^{+/+}$:HCVcpTg mice (Figure 4, A and B). In contrast, the number of TUNEL-positive hepatocytes and the hepatic caspase 3 activity, indicators of hepatocyte apoptosis, remained similar among the 3 mouse strains (Figure 4, C and D). Interestingly, despite the presence of HCV core protein, the amounts of these proliferative and apoptotic markers in *Ppara*$^{+/-}$:HCVcpTg and *Ppara*$^{-/-}$:HCVcpTg mice were similar to those in *Ppara*$^{+/+}$ nontransgenic mice. Expression levels of several proteins, such as protooncogenes (c-Fos and c-Myc), cell-cycle regulators (cyclin D1, cyclin-dependent kinase [CDK] 4, and PCNA), and phosphorylated ERK 1 and 2, all of which are associated with hepatocyte proliferation, were elevated in *Ppara*$^{+/+}$:HCVcpTg mice but not in other genotypes (Figure 4, E and F).

Increased oxidative stress and DNA damage only in Ppara$^{+/+}$*:HCVcpTg mice.* HCV core protein is associated with increased production of ROS (23). Enhanced ROS production induces nuclear DNA damage, which results in the initiation of hepatocarcinogenesis, and can also injure organelles, which can result in disorders in their

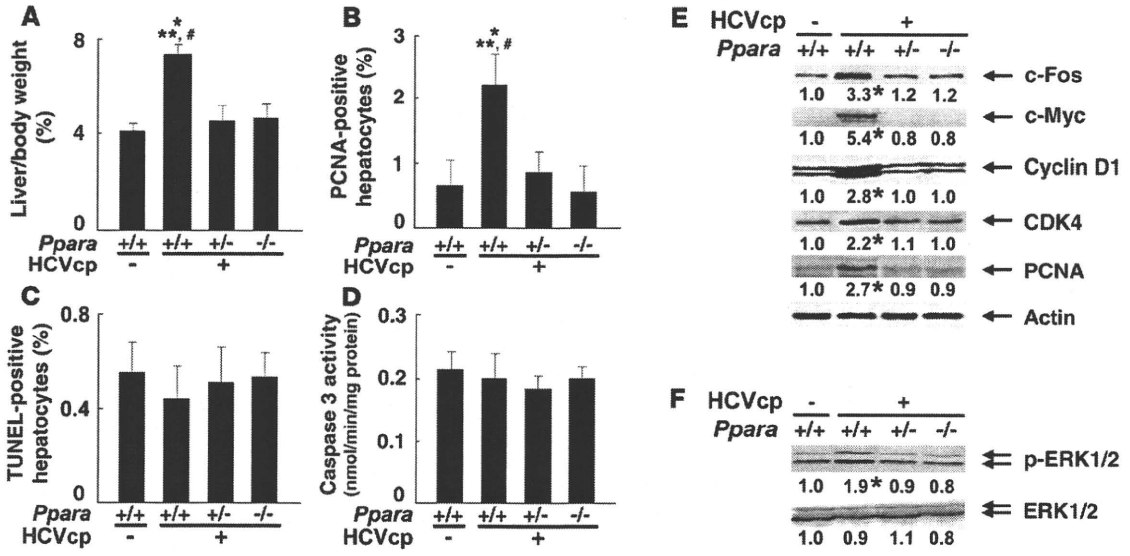

Figure 4
Increased hepatocyte proliferation in *Ppara*$^{+/+}$:HCVcpTg mice at 24 months of age. (**A**) Liver-to-body-weight ratio. Results are expressed as the mean ± SD (n = 6/group). (**B**) Numbers of proliferating hepatocytes. Two thousand hepatocytes were examined in each mouse, and hepatocyte nuclei positive for anti-PCNA antibody were counted. Results are expressed as the mean ± SD (n = 6/group). For **A** and **B**, comparisons are designated as follows: *$P < 0.05$ compared with *Ppara*$^{+/+}$ nontransgenic mice; **$P < 0.05$ compared with *Ppara*$^{+/-}$:HCVcpTg mice; #$P < 0.05$ compared with *Ppara*$^{-/-}$:HCVcpTg mice. (**C**) Numbers of apoptotic hepatocytes. Liver sections were subjected to TUNEL staining, and TUNEL-positive hepatocyte nuclei were counted in 2,000 hepatocytes from each mouse. Results are expressed as the mean ± SD (n = 6/group). (**D**) Caspase 3 activity. Results are expressed as the mean ± SD (n = 6/group). (**E**) Immunoblot analysis of oncogene products and cell cycle regulators. The same sample used in Figure 1A (whole-liver lysate, 50 μg protein) was loaded in each well. The band of actin was used as the loading control. Results are representative of 4 independent experiments. The band intensity was quantified densitometrically, normalized by that of actin, and subsequently normalized by that in *Ppara*$^{+/+}$ nontransgenic mice. The mean value of the fold changes is expressed under each band. (**F**) Immunoblot analysis of phosphorylated ERK1/2 and total ERK1/2. The same samples in Figure 4E (50 μg protein) were used.

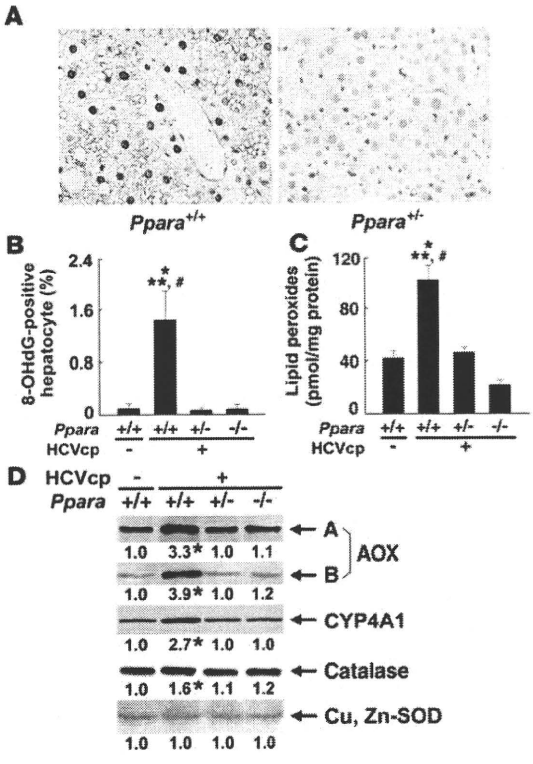

Figure 5
Increased oxidative stress and DNA damage in *Ppara*$^{+/+}$:HCVcpTg mice at 24 months of age. (**A**) Immunohistochemical staining using antibody against 8-OHdG. In *Ppara*$^{+/+}$:HCVcpTg mice, some steatotic hepatocytes were positive for 8-OHdG. Original magnification, ×400. (**B**) Numbers of 8-OHdG–positive hepatocytes. Hepatocyte nuclei stained with anti-8-OHdG antibody were counted in 2,000 hepatocytes of each mouse. Results are expressed as the mean ± SD (n = 6/group). (**C**) Hepatic content of lipid peroxides. Results are expressed as the mean ± SD (n = 6 /group). $^{*}P < 0.05$ compared with *Ppara*$^{+/+}$ nontransgenic mice; $^{**}P < 0.05$ compared with *Ppara*$^{+/-}$:HCVcpTg mice; $^{\#}P < 0.05$ compared with *Ppara*$^{-/-}$:HCVcpTg mice. (**D**) Immunoblot analysis of AOX, CYP4A1, catalase, and Cu, Zn-SOD. The whole-liver lysate used in the experiment in Figure 4E (20 μg protein for AOX and CYP4A1 and 50 μg for others) was loaded in each lane. The band of actin was used as the loading control. Results are representative of 4 independent experiments. **A** and **B** indicate full-length and truncated AOX, respectively. The band intensity was quantified densitometrically, normalized by that of actin, and subsequently normalized by that in *Ppara*$^{+/+}$ nontransgenic mice. The mean value of the fold changes is expressed under each band. $^{*}P < 0.05$ compared with *Ppara*$^{+/+}$ nontransgenic mice.

function. The number of hepatocytes positive for 8-hydroxy-2′-deoxyguanosine (8-OHdG), an indicator of oxidative damage to nuclear DNA, was increased only in 24-month-old *Ppara*$^{+/+}$:HCVcpTg mice (Figure 5, A and B). Lipid peroxides were slightly increased in the livers of 9-month-old *Ppara*$^{+/+}$:HCVcpTg mice (data not shown) and were more abundant in the livers of 24-month-old *Ppara*$^{+/+}$:HCVcpTg mice than in those of *Ppara*$^{+/-}$:HCVcpTg and *Ppara*$^{-/-}$:HCVcpTg mice or *Ppara*$^{+/+}$ nontransgenic mice (Figure 5C). Expression of typical ROS-generating enzymes (AOX and cytochrome P450 4A1 [CYP4A1]) and ROS-eliminating enzymes (catalase and Cu, Zn-SOD) was examined. Immunoblot analysis showed marked increases in the expression of AOX and CYP4A1 and mild increases in that of catalase only in *Ppara*$^{+/+}$:HCVcpTg mice. No changes in Cu, Zn-SOD were found in the subgroups of transgenic mice (Figure 5D). These results suggest that enhanced oxidative stress causes damage in nuclear DNA and probably in mitochondria in the *Ppara*$^{+/+}$:HCVcpTg mice.

Persistent and spontaneous PPARα activation in Ppara$^{+/+}$*:HCVcpTg mice.* Liver tumorigenesis induced by long-term exposure to peroxisome proliferators and the related changes, such as sustained hepatocyte proliferation and increased oxidative stress, are associated with persistent PPARα activation (19–21). To examine the activation of PPARα, we quantified the level of PPARα mRNA, which is induced by PPARα activation (24, 25). PPARα mRNA levels were higher in 9-month-old *Ppara*$^{+/+}$:HCVcpTg mice than in *Ppara*$^{+/+}$ nontransgenic mice (Figure 6A). These increases were more pronounced at 24 months of age. However, there were no differences in PPARα mRNA levels between *Ppara*$^{+/-}$:HCVcpTg and *Ppara*$^{+/-}$ nontransgenic mice at either 9 or 24 months of age. The expression levels of typical PPARα target genes (16, 25, 26) – such as FAT, FATP, L-FABP, AOX, and MCAD (Figure 2); c-Myc, cyclin D1, CDK4, and PCNA (Figure 4); and CYP4A1 (Figure 5) – were simultaneously and synchronously increased in *Ppara*$^{+/+}$:HCVcpTg mice, but not in *Ppara*$^{+/-}$:HCVcpTg or *Ppara*$^{-/-}$:HCVcpTg mice. These results confirm that persistent activation of PPARα occurs only in *Ppara*$^{+/+}$:HCVcpTg mice. Various changes observed in *Ppara*$^{+/+}$:HCVcpTg mice, i.e., increased fatty acid uptake, mitochondrial abnormalities, steatosis, ROS overproduction, accelerated hepatocyte proliferation, and hepatocarcinogenesis, were considered to be closely linked with sustained PPARα activation.

Nuclear PPARα content. The results described above suggest that persistent PPARα activation is critical to the steatogenesis and hepatocarcinogenesis induced by the HCV core protein. A question arises as to why *Ppara*$^{+/-}$:HCVcpTg mice with an active *Ppara* allele do not exhibit the hallmarks of PPARα activation and do not develop HCC. To address this issue, the nuclear PPARα content was analyzed. Immunoblot analysis for PPARα showed that the amount of nuclear PPARα protein in *Ppara*$^{+/+}$:HCVcpTg mice was approximately 2- to 3-fold that of *Ppara*$^{+/+}$ nontransgenic mice, which was disproportionate to the higher PPARα mRNA levels (approximately 1.2- to 1.6-fold) (Figure 6, A and B). The level of nuclear PPARα in *Ppara*$^{+/-}$:HCVcpTg mice was significantly lower than that in *Ppara*$^{+/+}$:HCVcpTg mice and was similar to that in *Ppara*$^{+/+}$ nontransgenic mice (Figure 6B). Thus, the lower amount of nuclear PPARα in *Ppara*$^{+/-}$:HCVcpTg mice than in *Ppara*$^{+/+}$:HCVcpTg mice might have heightened the threshold of expression required for long-term spontaneous PPARα activation.

The degree of an increase in nuclear PPARα levels was evidently higher than the degree of an increase in PPARα mRNA levels in HCVcpTg mice (Figure 6, A and B). To investigate this disparity, the stability of nuclear PPARα was evaluated by pulse-chase experiments using isolated hepatocytes obtained from these mice. The half-life of nuclear PPARα was significantly longer ($P < 0.05$) in *Ppara*$^{+/+}$:HCVcpTg mice (11.5 ± 2.3 h) than in *Ppara*$^{+/+}$ nontransgenic mice (5.8 ± 1.4 h) (Figure 6C). The half-life of nuclear PPARα in *Ppara*$^{+/-}$:HCVcpTg mice tended to be prolonged compared with that in *Ppara*$^{+/-}$ nontransgenic mice (Figure 6C). These results suggest that the stability of nuclear PPARα was increased as a result of HCV core protein expression. Because it is known that the core protein interacts with retinoid X receptor α (RXRα) (27) and that

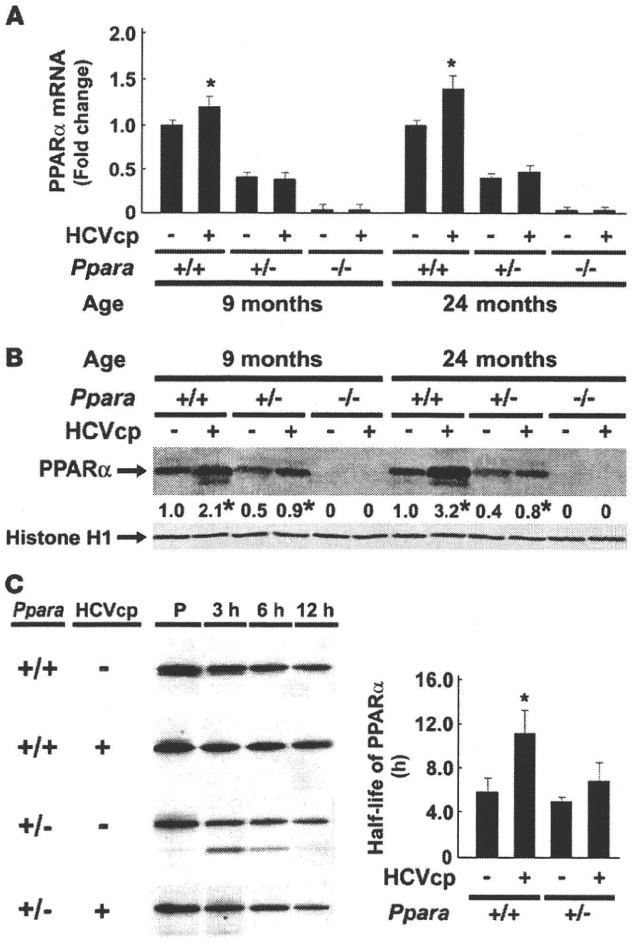

Figure 6

Persistent PPARα activation in *Ppara*$^{+/+}$:HCVcpTg mice. (**A**) PPARα mRNA levels. Total RNA was prepared from each mouse, and PPARα mRNA levels were determined by RT-PCR, normalized by those of GAPDH, and subsequently normalized by those of 9-month-old *Ppara*$^{+/+}$ nontransgenic mice. Results are expressed as the mean ± SD (n = 6 /group). (**B**) Immunoblot analysis of nuclear PPARα. The nuclear fraction obtained from each mouse (100 μg protein) was loaded in each well. The band of histone H1 was used as the loading control. Results are representative of 6 independent experiments. The band intensity was quantified densitometrically, normalized by that of histone H1, and subsequently normalized by that in 9-month-old *Ppara*$^{+/+}$ nontransgenic mice. The mean value is expressed under each band. *P < 0.05 compared with nontransgenic mice of the same age and *Ppara* genotype. (**C**) Pulse-chase experiments for 3, 6, and 12 h and pulse-label (P) experiments for nuclear PPARα using isolated mouse hepatocytes. Left: labeled PPARα bands on x-ray film. Pulse-label and pulse-chase experiments were performed as described in Methods. Results are representative of 4 independent experiments. Right: half-life of PPARα. The band intensity was measured densitometrically and subsequently normalized by that of the pulse-label experiments. The percentage of the band intensity was plotted, and the half-life of PPARα was calculated. Results obtained from 4 independent experiments are expressed as the mean ± SD. *P < 0.05 compared with nontransgenic mice in the same *Ppara* genotype.

PPARα influences the stability of RXRα (28), it is plausible that the core protein would affect its action in nuclei through an interaction with the PPARα-RXRα heterodimer and stabilization of PPARα.

Development of hepatic steatosis and HCC with long-term clofibrate treatment in Ppara$^{+/-}$*:HCVcpTg mice.* To further confirm the significance of persistent PPARα activation on core protein–induced pathological changes, *Ppara*$^{+/-}$ and *Ppara*$^{+/-}$:HCVcpTg mice were fed a standard diet containing 0.05% clofibrate for 24 months. Interestingly, hepatic steatosis appeared in the clofibrate-treated *Ppara*$^{+/-}$:HCVcpTg mice, but not in the *Ppara*$^{+/-}$ mice under the same treatment conditions (Figure 7, A and B). Similar to our observations in *Ppara*$^{+/+}$:HCVcpTg mice not treated with clofibrate, aberrant mitochondria with discontinuous outer membranes and decreased palmitic acid β-oxidation activity were found only in the clofibrate-treated *Ppara*$^{+/-}$:HCVcpTg mice (Figure 7, A and C). In addition, levels of MCAD mRNA; AOX, and CYP4A1 proteins; PPARα mRNA; and nuclear PPARα protein were higher in the clofibrate-treated *Ppara*$^{+/-}$:HCVcpTg mice than in the clofibrate-treated *Ppara*$^{+/-}$ mice (Figure 7, D–F), which suggests that the degree of PPARα activation in the former group was greater than that in the latter group and similar to that in *Ppara*$^{+/+}$:HCVcpTg mice not treated with clofibrate. Finally, the incidence of HCC after clofibrate treatment was higher in *Ppara*$^{+/-}$:HCVcpTg mice (25%; 5 in 20 mice) than in *Ppara*$^{+/-}$ mice (5%; 1 in 20 mice). Therefore, these results corroborate the importance of constant PPARα activation to the pathogenesis of hepatic steatosis and HCC in the transgenic mice.

Discussion

A novel and striking finding in this study is the absolute requirement of persistent PPARα activation for the development of HCV core protein–induced steatosis and HCC. Our data also show that the HCV core protein alone cannot induce steatosis and HCC in transgenic mice.

Mechanisms of development of steatosis in HCVcpTg mice were previously explained as an enhancement of de novo synthesis of fatty acids (29) and a decrease in MTP expression, the latter of which results in insufficient VLDL secretion from hepatocytes (30). In the present study, we revealed 2 novel mechanisms of steatogenesis in the transgenic mice, i.e., an impairment of mitochondrial β-oxidation due to the breakdown of mitochondrial outer membranes and an increase in fatty acid uptake into hepatocytes, associated with PPARα activation. PPARα activation, mitochondrial dysfunction, and hepatic steatosis appeared in 9-month-old *Ppara*$^{+/+}$:HCVcpTg mice and continued until 24 months of age, clearly preceding development of HCC. These findings thereby indicate a correlation between PPARα activation, hepatic steatosis, and HCC.

We obtained the novel and rather paradoxical finding that significant PPARα activation, which generally is expected to reduce hepatic triglyceride levels, is essential for the development of severe steatosis induced by HCV core protein. According to the results of this study, the following hypothesis concerning the development of steatosis in *Ppara*$^{+/+}$:HCVcpTg mice is proposed. First, the HCV core protein localizes partly in mitochondria (9). A recent study

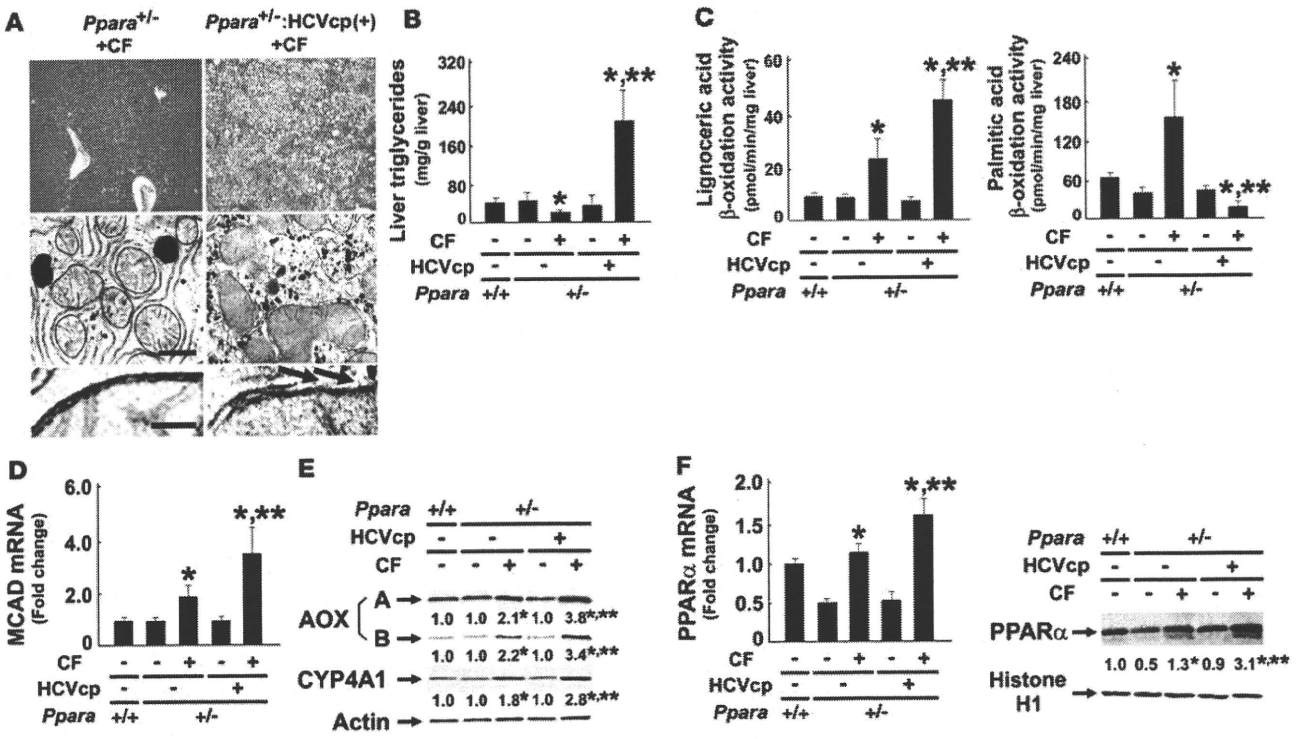

Figure 7

Development of hepatic steatosis by long-term treatment of clofibrate in *Ppara*$^{+/-}$:HCVcpTg mice. (**A**) Histological examination of *Ppara*$^{+/-}$ and *Ppara*$^{+/-}$:HCVcpTg mice treated with diet containing 0.05% (w/w) clofibrate for 24 months (CF). Top: Histological appearance of H&E-stained liver sections. Magnification, ×40. Microvesicular and macrovesicular steatosis were detected only in clofibrate-treated *Ppara*$^{+/-}$:HCVcpTg mice. Middle and bottom: Electron microscopic features of hepatic mitochondria. Some C-shaped mitochondria showing discontinuance of outer membranes (arrows) were found in clofibrate-treated *Ppara*$^{+/-}$:HCVcpTg mice. Scale bars: 400 nm (middle), 30 nm (bottom). (**B** and **C**) Content of liver triglycerides and lignoceric and palmitic acid β-oxidation activities. (**D**) MCAD mRNA levels. mRNA levels were normalized to those of GAPDH and subsequently normalized to those in *Ppara*$^{+/+}$ nontransgenic mice. (**E**) Immunoblot analysis of AOX and CYP4A1. Whole-liver lysate (20 μg protein) was loaded in each lane. Actin was used as a loading control. Results are representative of 6 independent experiments. (**F**) PPARα mRNA levels and nuclear PPARα contents. Left: PPARα mRNA levels. The same samples used in **D** were adopted. Right: Immunoblot analysis of nuclear PPARα. Nuclear fraction obtained from each mouse (100 μg protein) was loaded in each well. Histone H1 was used as a loading control. In **E** and **F**, the mean value of the fold changes is shown under each band. Results are representative of 6 independent experiments. Band intensity was quantified densitometrically, normalized to that of the loading control, and subsequently normalized to that in *Ppara*$^{+/+}$ nontransgenic mice. *$P < 0.05$ compared with untreated mice of the same genotype; **$P < 0.05$ compared with clofibrate-treated *Ppara*$^{+/-}$ mice without core protein gene. Results are expressed as mean ± SD (n = 6/group).

showed that, in isolated mitochondria, the core protein directly increased Ca^{2+} influx, inhibited electron transport complex I activity, and induced ROS production (31), all of which can increase the fragility of mitochondria and depress mitochondrial function. In addition, the HCV core protein also localizes in nuclei (9) and can coexist in PPARα-RXRα heterodimer through a direct interaction with the DNA-binding domain of RXRα, which enhances the transcriptional activity of PPARα target genes, such as AOX, despite the absence of PPARα ligands in cultured cells (27). The HCV core protein can also be involved in the PPARα-RXRα complex through a direct interaction with cyclic-AMP responsive element binding protein-binding protein (32), which is able to bind to PPARα (33). Thus, the core protein probably serves as a coactivator and stabilizer of PPARα in vivo, which was further confirmed in this study. Moreover, because it is also known that the core protein itself activates ERK1/2 and p38 mitogen-activated protein kinase (34), these activations might phosphorylate PPARα and thereby transactivate it (35). The core protein–induced PPARα activation enhances the basal expression of AOX and CYP4A1, which leads to increased production of ROS and dicarboxylic acids. These toxic compounds can damage mitochondrial outer membranes, which impairs the mitochondrial β-oxidation system. These damages directly induce the accumulation of long-chain fatty acids in hepatocytes. Furthermore, PPARα activation increases the expression of FAT and FATP, which promotes the influx of fatty acids from blood. Long-chain fatty acids and their CoA esters accumulated in hepatocytes are likely to act as potent detergents, which further damages the outer membranes of mitochondria. Fatty acids and their derivatives function as natural ligands of PPARα, which results in the activation of PPARα and the induction of FAT, FATP, AOX, and CYP4A1, which further accelerates mitochondrial damage, the reduction of mitochondrial β-oxidation activity, and the accumulation of fatty acids in a vicious cycle.

Persistent PPARα activation increases oxidative DNA damage because of a disproportionate increase in ROS-generating enzymes relative to the levels of degrading enzymes such as catalase and SOD, which can predispose hepatocytes to malignant transformation. In addition, persistent PPARα activation leads to increased

Table 2
Primer pairs used for RT-PCR

Gene	GeneBank accession number		Primer sequence	Product (bp)
ACC	NM_133360	F	5′-GGGCACAGACCGTGGTAGTT-3′	105
		R	5′-CAGGATCAGCTGGGATACTGAGT-3′	
ApoB	NM_009693	F	5′-TCACCCCCGGGATCAAG-3′	85
		R	5′-TCCAAGGACACAGAGGGCTTT-3′	
AOX	NM_015729	F	5′-TGGTATGGTGTCGTACTTGAATGAC-3′	145
		R	5′-AATTTCTACCAATCTGGCTGCAC-3′	
FAS	NM_007988	F	5′-ATCCTGGAACGAGAACACGATCT-3′	140
		R	5′-AGAGACGTGTCACTCCTGGACTT-3′	
FAT	NM_007643	F	5′-CCAAATGAAGATGAGCATAGGACAT-3′	87
		R	5′-GTTGACCTGCAGTCGTTTTGC-3′	
FATP	NM_011977	F	5′-ACCACCGGGCTTCCTAAGG-3′	80
		R	5′-CTGTAGGAATGGTGGCCAAAG-3′	
GAPDH	M32599	F	5′-TGCACCACCAACTGCTTAG-3′	177
		R	5′-GGATGCAGGGATGATGTTCTG-3′	
L-FABP	NM_017399	F	5′-GCAGAGCCAGGAGAACTTTGAG-3′	121
		R	5′-TTTGATTTTCTTCCCTTCATGCA-3′	
MCAD	NM_007382	F	5′-TGCTTTTGATAGAACCAGACCTACAGT-3′	128
		R	5′-CTTGGTGCTCCACTAGCAGCTT-3′	
MTP	NM_008642	F	5′-GAGCGGTCTGGATTTACAACG-3′	72
		R	5′-GTAGGTAGTGACAGATGTGGCTTTTG-3′	
PPARα	NM_011144	F	5′-CCTCAGGGTACCACTACGGAGT-3′	69
		R	5′-GCCGAATAGTTCGCCGAA-3′	

F, forward sequence; R, reverse sequence.

cell division, as revealed by the expression of cell cycle regulators such as cyclin D1 and CDK4. Furthermore, there is little change in apoptosis, which, under normal circumstances, would remove damaged cells capable of undergoing transformation. Thus, under these conditions, it is plausible that some aberrant hepatocytes do not undergo apoptosis and develop into HCC.

It is well known that chronic activation of PPARα is associated with hepatocarcinogenesis in mice exposed to peroxisome proliferators or in mice lacking AOX expression. The common clinicopathological characteristics of HCC in these mice are multicentric HCC (20, 22, 36, 37), the well-differentiated appearance of HCC including trabecular features and often a "nodule-in-nodule" pattern (22, 36, 37), and no evidence of fibrosis or cirrhosis in the nonneoplastic liver parenchyma (22, 36), similar to that observed in *Ppara*$^{+/+}$:HCVcpTg mice. However, mice chronically exposed to peroxisome proliferators are clearly distinct from *Ppara*$^{+/+}$:HCVcpTg mice in that they have normal mitochondrial organization, increased mitochondrial β-oxidation activity, and no steatosis (16, 36). AOX-null mice are also different from *Ppara*$^{+/+}$:HCVcpTg mice with respect to mitochondrial structure (22). These detailed comparisons between the 3 mouse models reveal the importance of mitochondrial abnormalities in the pathogenesis of HCV-related diseases.

PPARα is known to regulate the hepatic expression of many proteins associated with fatty acid and triglyceride metabolism, cell division and apoptosis, oxidative stress generation and degradation, and so forth (15, 16, 20, 21, 24–26); therefore, complete deletion of the PPARα gene from mice might cause hitherto unknown influences on the pathways involved in the development of hepatic steatosis and HCC. To consider these unknown effects, *Ppara*$^{+/-}$:HCVcpTg mice were adopted in the current study. Surprisingly, almost all results from *Ppara*$^{+/-}$:HCVcpTg mice were similar to those from *Ppara*$^{-/-}$:HCVcpTg mice, which demonstrates that the presence of functional PPARα itself is not a prerequisite for the occurrence of steatosis and HCC induced by the HCV core protein. Moreover, a comparison between *Ppara*$^{+/-}$:HCVcpTg and *Ppara*$^{+/+}$:HCVcpTg mice uncovered an unexpected and important fact that the core protein–dependent pathological changes do not appear without significant activation of PPARα. Thus, it is not the presence of PPARα per se, but rather a high level of PPARα activation that seems to be essential for the development of HCV core protein–induced steatosis and HCC.

To reinforce the abovementioned hypothesis, *Ppara*$^{+/-}$ and *Ppara*$^{+/-}$:HCVcpTg mice were treated with an exogenous PPAR agonist, clofibrate, for 24 months. In *Ppara*$^{+/-}$ mice, long-term clofibrate treatment caused a certain level of persistent PPARα activation and a low incidence of HCC. Interestingly, in *Ppara*$^{+/-}$:HCVcpTg mice, clofibrate treatment induced more intensive PPARα activation and HCC at a much higher incidence, accompanied by damaged mitochondrial outer membranes, severe steatosis, and decreased mitochondrial β-oxidation activity. The results from the clofibrate-treated *Ppara*$^{+/-}$:HCVcpTg mice were similar to those of the *Ppara*$^{+/+}$:HCVcpTg mice not treated with clofibrate. Therefore, these findings further support the concept that a long-term and high level of PPARα activation is necessary for steatogenesis and hepatocarcinogenesis in HCVcpTg mice and emphasize the significant role of the HCV core protein as a PPARα coactivator in vivo.

A pulse-chase experiment showed that PPARα was stabilized in hepatocyte nuclei in mice expressing the HCV core protein. Many nuclear receptors, including PPARα and RXRα, are known to be degraded by the ubiquitin-proteasome system (38), which plays an important role in modulating the activity of nuclear receptors. Further studies will be needed to clarify whether the core protein influences the ubiquitin-proteasome pathway.

Recent studies have shown conflicting result, i.e., that PPARα was downregulated in the livers of chronic hepatitis C patients (39, 40). Although the association between PPARα function and chronic HCV infection remains a matter of controversy in humans, the changes observed in the transgenic mice resemble in many ways the clinicopathological features of chronically HCV-infected patients; both show a high frequency of accompanying steatosis (10, 40, 41), increased accumulation of carbon 18 monounsaturated fatty acids in the liver (42), mitochondrial dysfunction (43), increased insulin resistance (44) and oxidative stress (45, 46), male-preferential (2) and multicentric occurrence of HCC (47, 48), and the well-differentiated appearance of HCC, including trabecular features and often a "nodule-in-nodule" pattern (47, 48). Thus, it is postulated that the mechanism of steatogenesis and hepatocarcinogenesis we proposed may partially apply to patients with chronic HCV infection. If so, therapeutic interventions to alleviate persistent and excessive PPARα activation might be beneficial in the prevention of HCC. To clarify the exact relationship between PPARα activation and HCV-induced hepatocarcinogenesis in humans, further

experiments using noncancerous liver tissues obtained from HCV-related HCC patients and using mice carrying human PPARα and HCV core protein genes are needed.

In conclusion, we clarified for the first time that persistent and potent PPARα activation is absolutely required for the development of severe steatosis and HCC induced by HCV core protein. In addition, we uncovered paradoxical and specific functions of PPARα in the mechanism of steatogenesis mediated by the core protein. Our results offer clues in the search for novel therapeutic and nutritional management options, especially with respect to neutral lipids, for chronically HCV-infected patients.

Methods

Mice. The generation of HCVcpTg mice and *Ppara*$^{-/-}$ mice was described previously (7, 24, 49). Male HCVcpTg mice and female *Ppara*$^{-/-}$ mice were mated, and F1 mice bearing the HCV core protein gene were intercrossed to produce F2 mice. *Ppara*$^{+/+}$, *Ppara*$^{+/-}$, and *Ppara*$^{-/-}$ mice bearing the HCV core protein gene, designated as *Ppara*$^{+/+}$:HCVcpTg, *Ppara*$^{+/-}$:HCVcpTg, and *Ppara*$^{-/-}$:HCVcpTg mice, in the F4 generation were subjected to serial analyses. Because HCC develops preferentially in male HCVcpTg mice (9), male mice were analyzed. Age-matched male *Ppara*$^{+/+}$ mice without the core protein gene were used as controls. For identifying genotypes, genomic DNA was isolated from mouse tails and amplified by PCR. Primer pairs were designed as described elsewhere: 5′-GCCCACAGGACGTTAAGTTC-3′ and 5′-TAGTTCACGCCGTCCTCCAG-3′ for the HCV core gene (7) and 5′-CAGAGCAACCATCCAGATGA-3′ and 5′-AAACGCAACGTAGAGTGCTG-3′ for the PPARα gene (24). Amplified alleles for HCV core and PPARα genes were 460 and 472 base pairs, respectively. Five mice per cage were fed a routine diet and were kept free of specific pathogens according to institutional guidelines. For the clofibrate treatment experiments, 2-month-old male *Ppara*$^{+/-}$ and *Ppara*$^{+/-}$:HCVcpTg mice were randomly divided into 2 groups (n = 20 in each group) and were fed either a routine diet or one containing 0.05% (w/w) clofibrate (Wako Pure Chemicals Industries) for 24 months. All mice were killed by cervical dislocation before their livers were excised. If a hepatic tumor was present, the tumor was removed and subjected to histological analysis, and the remaining liver tissues were used for biochemical analyses. All animal experiments were conducted in accordance with animal study protocols outlined in the *Guide for the Care and Use of Laboratory Animals* prepared by the National Academy of Sciences and approved by the Shinshu University School of Medicine.

Preparation of nuclear, mitochondrial, and cytosolic fractions. Approximately 400 mg of liver tissue was minced on ice and transferred to 10% (w/v) isolation buffer (250 mM sucrose in 10 mM Tris-HCl [pH 7.4] and 0.5 mM EGTA and 0.1% bovine serum albumin [pH 7.4]). The samples were gently homogenized by 10–20 strokes with a chilled Dounce homogenizer (Wheaton) and loose-fitting pestle. The homogenate was centrifuged at 500 × *g* for 5 min at 4°C. The supernatant was retained, and the resulting pellet was resuspended with isolation buffer and centrifuged at 4,500 *g* for 10 min at 4°C. The pellet fraction was suspended again and centrifuged at 20,000 × *g* for 1 h at 4°C, and the resulting pellet was used as the nuclear fraction. The combined supernatant fractions were centrifuged at 7,800 × *g* for 10 min at 4°C to obtain a crude mitochondria pellet. This pellet was resuspended with isolation buffer, centrifuged at 7,800 × *g* for 10 min at 4°C, and used as the mitochondrial fraction. Finally, all supernatant fractions were collected and centrifuged at 20,000 × *g* for 30 min at 4°C, and the resulting supernatant was used as the cytosolic fraction.

Immunoblot analysis. Protein concentrations were measured colorimetrically with a BCA Protein Assay kit (Pierce). For the analysis of fatty acid–metabolizing enzymes, hepatocyte mitochondrial fractions or whole-liver lysates (20 μg protein) were subjected to 10% SDS-PAGE (16). For analysis of PPARα, nuclear fractions (100 μg protein) were used. For analysis of other proteins, whole lysates or cytosolic fractions (50 μg protein) were subjected to electrophoresis. After electrophoresis, the proteins were transferred to nitrocellulose membranes, which were incubated with the primary antibody and then with alkaline phosphatase-conjugated goat anti-rabbit or anti-mouse IgG. Antibodies against HCV core protein, fatty acid–metabolizing enzymes, CYP4A1, catalase, and PPARα were described previously (9, 16, 24, 50). Antibodies against other proteins were purchased commercially: cytochrome *c* antibody from BD Transduction Laboratories and other antibodies from Santa Cruz Biotechnology. The band of actin or histone H1 was used as the loading control. The band intensity was measured densitometrically, normalized to that of actin or histone H1, and subsequently expressed as fold changes relative to that of *Ppara*$^{+/+}$ nontransgenic mice.

Analysis of mRNA. Total liver RNA was extracted using an RNeasy Mini Kit (Qiagen), and cDNA was generated by SuperScript II reverse transcriptase (Gibco BRL). Quantitative RT-PCR was performed using a SYBR green PCR kit and an ABI Prism 7700 Sequence Detection System (Applied Biosystems). The primer pairs used for RT-PCR are shown in Table 2. The mRNA level was normalized to the GAPDH mRNA level and subsequently expressed as fold changes relative to that of *Ppara*$^{+/+}$ nontransgenic mice.

Light microscopy and immunohistochemical analysis. Small blocks of liver tissue from each mouse were fixed in 10% formalin in phosphate-buffered saline and embedded in paraffin. Sections (4 μm thick) were stained with hematoxylin and eosin. For immunohistochemical localization of PCNA and 8-OHdG, other small blocks of liver tissue were fixed in 4% paraformaldehyde in phosphate-buffered saline. Sections (4 μm thick) then were affixed to glass slides and incubated overnight with mouse monoclonal antibodies against PCNA (1:100 dilution; Santa Cruz) or 8-OHdG (1:10 dilution; Japan Institute for the Control of Aging). Sections were immunostained using EnVision+ kit, with 3,3′-diaminobenzidine as a substrate (DAKO). Hepatocytes positive for PCNA or 8-OHdG were examined in 10 randomly selected ×400 microscopic fields per section. Two-thousand hepatocytes were examined for each mouse, and the number of immunostained hepatocyte nuclei was expressed as a percentage.

Assessment of hepatocyte apoptosis. TUNEL assay was performed using a MEBSTAIN Apoptosis Kit II (Medical & Biological Laboratories). Two thousand hepatocytes were examined for each mouse, and the number of TUNEL-positive hepatocytes was expressed as a percentage.

Pulse-label and pulse-chase experiments. Parenchymal hepatocytes were isolated by the modified *in situ* perfusion method (51). After perfusion with 0.05% collagenase solution (Wako), the isolated hepatocytes were washed 3 times by means of differential centrifugation and the dead cells were removed by density-gradient centrifugation at 500 *g* for 3 min at 4°C on Percoll (Amersham Pharmacia Biotech). The live hepatocytes were washed and suspended in William's E medium containing 5% FBS. When the viability of the isolated hepatocytes exceeded 85% as determined by the trypan blue exclusion test, the following experiments were conducted. The isolated hepatocytes were washed twice and incubated in methionine-free medium containing 5% dialyzed FBS for 1 h at 37°C. The medium was replaced with the same medium containing 300 mCi/ml of [^{35}S]methionine (Amersham Pharmacia Biotech). After a 3-h incubation, the labeled medium was exchanged for the standard medium, and the preparation was chased for 3, 6, or 12 h. The labeled cells were washed, homogenized, and centrifuged at 800 *g* for 5 min at 4°C to obtain a crude nucleus pellet. This pellet was resuspended with isolation buffer and centrifuged at 20,000 *g* for 1 h at 4°C to prepare the nuclear fraction. The levels of radioactivity in the homogenates of the pulse-labeled preparations were similar between the transgenic and the nontransgenic mice, which suggested that the [^{35}S]methionine uptake capacity in the former hepatocytes was similar to that in the latter. The nuclear fraction was lysed in RIPA buffer (10 mM Tris-HCl, pH 7.4; 0.2% sodium deoxycholate, 0.2% Nonidet P-40, 0.1% SDS,

0.25 mM PMSF, and 10 mg/ml aprotinin). The lysate was incubated for 3 h at 4°C with purified anti-PPARα antibody. The immune complexes were precipitated with *Staphylococcus aureus* protein A bound to agarose beads. After the precipitates had been washed in RIPA buffer, the labeled proteins were resolved by 10% SDS-PAGE and visualized by autoradiography.

Analysis of fatty acid uptake ability. Assays for fatty acid uptake were carried out according to a method reported by Graulet et al. (52) with minor modifications. Briefly, 3 mice in each group were fasted overnight. Livers were removed quickly, rinsed in ice-cold saline solution, and cut into 500-μm thick slices with an Oxford Vibratome (Oxford Laboratories). Approximately 150 mg of fresh liver (6–8 liver slices) was placed on stainless steel grids positioned in a 25-ml flask equipped with suspended plastic center wells (Kontes) and incubated in RPMI-1640 medium (Sigma-Aldrich) devoid of fatty acids for 2 h at 37°C. The medium was then replaced with fresh RPMI-1640 medium supplemented with an antibiotic-antimycotic cocktail and 0.8 mM [1-^{14}C]palmitic acid (4 mCi/mmol) (American Radiolabeled Chemicals) complexed to BSA (palmitic acid:albumin molar ratio of 4:1). After a 7-h incubation, the medium was collected and slices were washed with 2 ml of saline solution and homogenized in Tris buffer (25 mM Tris-HCl, pH 8.0; 50 mM NaCl). Fatty acid uptake ability was calculated as the sum of palmitic acid converted to CO_2 and ketone bodies with that incorporated into total cellular lipids after incubation. For measurement of CO_2 production by the liver slices, the center wells were placed into scintillation vials containing 4 ml of scintillation cocktail, and radioactivity was counted. For measurement of ketone body generation, aliquots of medium (500 μl) and liver homogenates (250 μl) were treated with ice-cold perchloric acid to make final concentrations of 200 mM and were centrifuged at 3,000 *g* for 20 min at 4°C. Aliquots of the supernatant containing the ketone bodies were introduced into the scintillation vials, and radioactivity was counted. Total cellular lipids were extracted from the liver homogenates according to a modified method developed by Folch et al. (53), collected into scintillation vials, and evaporated to dryness under an air stream; radioactivity was then counted. The experiment was repeated 3 times, and palmitic acid uptake ability was expressed as fold changes relative to that of *Ppara*$^{+/+}$ nontransgenic mice.

Other methods. To determine the hepatic content of lipids and lipid peroxides, lipids were extracted according to a method by Folch et al. (53). Triglycerides and free fatty acids were measured with a Triglyceride E-test kit and a NEFA C-test kit (Wako), respectively. Lipid peroxides (malondialdeyde and 4-hydroxyalkenals) were measured using an LPO-586 kit (OXIS International). Hepatic β-oxidation activity was determined as described previously (16). Hepatic caspase 3 activity was measured as described elsewhere (54). Plasma glucose and insulin levels were determined using a Glucose CII-test kit (Wako) and a mouse insulin ELISA kit (U-type, AKRIN-031; Shibayagi), respectively.

Statistics. Statistical analysis was performed with a 2-tailed Student's *t* test for quantitative variables or with a chi-square test for qualitative variables. Quantitative data are expressed as the mean ± SD. $P < 0.05$ was considered to be statistically significant.

Acknowledgments

We thank Trevor Ralph for editorial assistance and Chikako Tanaka for helpful suggestions.

Received for publication August 13, 2007, and accepted in revised form November 7, 2007.

Address correspondence to: Naoki Tanaka, Department of Metabolic Regulation, Institute on Aging and Adaptation, Shinshu University Graduate School of Medicine, Asahi 3-1-1, Matsumoto 390-8621, Japan. Phone: 81-263-37-2850; Fax: 81-263-37-3094; E-mail: naopi@hsp.md.shinshu-u.ac.jp.

1. Kiyosawa, K., et al. 1990. Interrelationship of blood transfusion, non-A, non-B hepatitis and hepatocellular carcinoma: analysis by detection of antibody to hepatitis C virus. *Hepatology.* **12**:671–675.
2. Kiyosawa, K., et al. 2004. Hepatocellular carcinoma: recent trends in Japan. *Gastroenterology.* **127**(5 Suppl. 1):S17–S26.
3. Tanaka, Y., et al. 2002. Inaugural article: a comparison of the molecular clock of hepatitis C virus in the United States and Japan predicts that hepatocellular carcinoma incidence in the United States will increase over the next two decades. *Proc. Natl. Acad. Sci. U. S. A.* **99**:15584–15589.
4. Okuda, K., Fujimoto, I., Hanai, A., and Urano, Y. 1987. Changing incidence of hepatocellular carcinoma in Japan. *Cancer Res.* **47**:4967–4972.
5. El-Serag, H.B., and Mason, A.C. 1999. Rising incidence of hepatocellular carcinoma in the United States. *N. Engl. J. Med.* **340**:745–750.
6. Shimotohno, K. 2000. Hepatitis C virus and its pathogenesis. *Semin. Cancer Biol.* **10**:233–240.
7. Moriya, K., et al. 1997. Hepatitis C virus core protein induces hepatic steatosis in transgenic mice. *J. Gen. Virol.* **78**:1527–1531.
8. Shintani, Y., et al. 2004. Hepatitis C virus infection and diabetes: direct involvement of the virus in the development of insulin resistance. *Gastroenterology.* **126**:840–848.
9. Moriya, K., et al. 1998. The core protein of hepatitis C virus induces hepatocellular carcinoma in transgenic mice. *Nat. Med.* **4**:1065–1068.
10. Powell, E.E., Jonsson, J.R., and Clouston, A.D. 2005. Steatosis: co-factor in other liver diseases. *Hepatology.* **42**:5–13.
11. Ohata, K., et al. 2003. Hepatic steatosis is a risk factor for hepatocellular carcinoma in patients with chronic hepatitis C virus infection. *Cancer.* **97**:3036–3043.
12. Browning, J.D., and Horton, J.D. 2004. Molecular mediators of hepatic steatosis and liver injury. *J. Clin. Invest.* **114**:147–152.
13. Le, T.H., et al. 2004. The zonal distribution of megamitochondria with crystalline inclusions in nonalcoholic steatohepatitis. *Hepatology.* **39**:1423–1429.
14. Yang, S., Lin, H.Z., Hwang, J., Chacko, V.P., and Diehl, A.M. 2001. Hepatic hyperplasia in noncirrhotic fatty livers: is obesity-related hepatic steatosis a premalignant condition? *Cancer Res.* **61**:5016–5023.
15. Desvergne, B., and Wahli, W. 1999. Peroxisome proliferator-activated receptors: nuclear control of metabolism. *Endocr. Rev.* **20**:649–688.
16. Aoyama, T., et al. 1998. Altered constitutive expression of fatty acid-metabolizing enzymes in mice lacking the peroxisome proliferator-activated receptor α (PPARα). *J. Biol. Chem.* **273**:5678–5684.
17. Staels, B., et al. 1998. Mechanism of action of fibrates on lipid and lipoprotein metabolism. *Circulation.* **98**:2088–2093.
18. Harano, Y., et al. 2006. Fenofibrate, a peroxisome proliferator-activated receptor α agonist, reduces hepatic steatosis and lipid peroxidation in fatty liver Shionogi mice with hereditary fatty liver. *Liver Int.* **26**:613–620.
19. Yeldandi, A.V., Rao, M.S., and Reddy, J.K. 2000. Hydrogen peroxide generation in peroxisome proliferator-induced oncogenesis. *Mutat. Res.* **448**:159–177.
20. Yu, S., Rao, M.S., and Reddy, J.K. 2003. Peroxisome proliferator-activated receptors, fatty acid oxidation, steatohepatitis and hepatocarcinogenesis. *Curr. Mol. Med.* **3**:561–572.
21. Peters, J.M., Cattley, R.C., and Gonzalez, F.J. 1997. Role of PPARα in the mechanism of action of the nongenotoxic carcinogen and peroxisome proliferator Wy-14,643. *Carcinogenesis.* **18**:2029–2033.
22. Fan, C.Y., et al. 1998. Steatohepatitis, spontaneous peroxisome proliferation and liver tumors in mice lacking peroxisomal fatty acyl-CoA oxidase. Implications for peroxisome proliferator-activated receptor α natural ligand metabolism. *J. Biol. Chem.* **273**:15639–15645.
23. Moriya, K., et al. 2001. Oxidative stress in the absence of inflammation in a mouse model for hepatitis C virus-associated hepatocarcinogenesis. *Cancer Res.* **61**:4365–4370.
24. Lee, S.S., et al. 1995. Targeted disruption of the α isoform of the peroxisome proliferator-activated receptor gene in mice results in abolishment of the pleiotropic effects of peroxisome proliferators. *Mol. Cell. Biol.* **15**:3012–3022.
25. Mandard, S., Muller, M., and Kersten, S. 2004. Peroxisome proliferator-activated receptor α target genes. *Cell. Mol. Life Sci.* **61**:393–416.
26. Peters, J.M., et al. 1998. Role of peroxisome proliferator-activated receptor α in altered cell cycle regulation in mouse liver. *Carcinogenesis.* **19**:1989–1994.
27. Tsutsumi, T., et al. 2002. Interaction of hepatitis C virus core protein with retinoid X receptor α modulates its transcriptional activity. *Hepatology.* **35**:937–946.
28. Tanaka, N., et al. 2003. In vivo stabilization of nuclear retinoid X receptor α in the presence of peroxisome proliferator-activated receptor α. *FEBS Lett.* **543**:120–124.
29. Moriishi, K., et al. 2007. Critical role of PA28γ in hepatitis C virus-associated steatogenesis and hepatocarcinogenesis. *Proc. Natl. Acad. Sci. U. S. A.* **104**:1661–1666.
30. Perlemuter, G., et al. 2002. Hepatitis C virus core

protein inhibits microsomal triglyceride transfer protein activity and very low density lipoprotein secretion: a model of viral-related steatosis. *FASEB J.* **16**:185–194.
31. Korenaga, M., et al. 2005. Hepatitis C virus core protein inhibits mitochondrial electron transport and increases reactive oxygen species (ROS) production. *J. Biol. Chem.* **280**:37481–37488.
32. Gomez-Gonzalo, M., et al. 2004. Hepatitis C virus core protein regulates p300/CBP co-activation function. Possible role in the regulation of NF-AT1 transcriptional activity. *Virology.* **328**:120–130.
33. Yu, S., and Reddy, J.K. 2007. Transcription coactivators for peroxisome proliferator-activated receptors. *Biochim. Biophys. Acta.* **1771**:936–951.
34. Spaziani, A., Alisi, A., Sanna, D., and Balsano, C. 2006. Role of p38 MAPK and RNA-dependent protein kinase (PKR) in hepatitis C virus core-dependent nuclear delocalization of cyclin B1. *J. Biol. Chem.* **281**:10983–10989.
35. Diradourian, C., Girard, J., and Pegorier, J.P. 2005. Phosphorylation of PPARs: from molecular characterization to physiological relevance. *Biochimie.* **87**:33–38.
36. Reddy, J.K., Rao, M.S., Azarnoff, D.L., and Sell, S. 1979. Mitogenic and carcinogenic effects of a hypolipidemic peroxisome proliferator, [4-chloro-6-(2,3-xylidino)-2- pyrimidinylthio]acetic acid (Wy-14,643), in rat and mouse liver. *Cancer Res.* **39**:152–161.
37. Rao, M.S., and Reddy, J.K. 1996. Hepatocarcinogenesis of peroxisome proliferators. *Ann. N. Y. Acad. Sci.* **804**:573–587.
38. Genini, D., and Catapano, C.V. 2006. Control of peroxisome proliferator-activated receptor fate by the ubiquitin-proteasome system. *J. Recept. Signal. Transduct. Res.* **26**:679–692.
39. Dharancy, S., et al. 2005. Impaired expression of the peroxisome proliferator-activated receptor alpha during hepatitis C virus infection. *Gastroenterology.* **128**:334–342.
40. de Gottardi, A., et al. 2006. Peroxisome proliferator-activated receptor-alpha and -gamma mRNA levels are reduced in chronic hepatitis C with steatosis and genotype 3 infection. *Aliment. Pharmacol. Ther.* **23**:107–114.
41. Lefkowitch, J.H., et al. 1993. Pathological diagnosis of chronic hepatitis C: a multicenter comparative study with chronic hepatitis B. *Gastroenterology.* **104**:595–603.
42. Moriya, K., et al. 2001. Increase in the concentration of carbon 18 monounsaturated fatty acids in the liver with hepatitis C: analysis in transgenic mice and humans. *Biochem. Biophys. Res. Commun.* **281**:1207–1212.
43. Barbaro, G., et al. 1999. Hepatocellular mitochondrial alterations in patients with chronic hepatitis C: ultrastructural and biochemical findings. *Am. J. Gastroenterol.* **94**:2198–2205.
44. Hui, J.M., et al. 2003. Insulin resistance is associated with chronic hepatitis C virus infection and fibrosis progression [corrected]. *Gastroenterology.* **125**:1695–1704.
45. Kato, J., et al. 2001. Normalization of elevated hepatic 8-hydroxy-2'-deoxyguanosine levels in chronic hepatitis C patients by phlebotomy and low iron diet. *Cancer Res.* **61**:8697–8702.
46. Horiike, S., et al. 2005. Accumulation of 8-nitroguanine in the liver of patients with chronic hepatitis C. *J. Hepatol.* **43**:403–410.
47. Takenaka, K., et al. 1994. Possible multicentric occurrence of hepatocellular carcinoma: a clinicopathological study. *Hepatology.* **19**:889–894.
48. Oikawa, T., et al. 2005. Multistep and multicentric development of hepatocellular carcinoma: histological analysis of 980 resected nodules. *J. Hepatol.* **42**:225–229.
49. Akiyama, T.E., et al. 2001. Peroxisome proliferator-activated receptor-α regulates lipid homeostasis, but is not associated with obesity. *J. Biol. Chem.* **276**:39088–39093.
50. Nakajima, T., et al. 2004. Peroxisome proliferator-activated receptor α protects against alcohol-induced liver damage. *Hepatology.* **40**:972–980.
51. Ni, R., et al. 1994. Fas-mediated apoptosis in primary cultured mouse hepatocytes. *Exp. Cell Res.* **215**:332–337.
52. Graulet, B., Gruffat, D., Durand, D., and Bauchart, D. 1998. Fatty acid metabolism and very low density lipoprotein secretion in liver slices from rats and preruminant calves. *J. Biochem.* **124**:1212–1219.
53. Folch, J., Lees, M., and Sloane Stanley, G.H. 1957. A simple method for the isolation and purification of total lipids from animal tissues. *J. Biol. Chem.* **226**:497–509.
54. Gurtu, V., Kain, S.R., and Zhang, G. 1997. Fluorometric and colorimetric detection of caspase activity associated with apoptosis. *Anal. Biochem.* **251**:98–102.

Practical cell-free protein synthesis system using purified wheat embryos

Kazuyuki Takai, Tatsuya Sawasaki & Yaeta Endo

Cell-Free Science and Technology Research Center and Venture Business Laboratory, Ehime University, Matsuyama, Japan. Correspondence should be addressed to Y.E. (yendo@eng.ehime-u.ac.jp).

Published online 21 January 2010; doi:10.1038/nprot.2009.207

Biochemical characterization of each gene product encoded in the genome is essential to understand how cells are regulated. The bottleneck has been and still is in how the gene products can be obtained. The wheat cell-free protein synthesis system we have developed is a powerful method for preparation of many different proteins at a time and also for preparation of large amounts of specific proteins for biochemical and structural analyses. Here, we show a method for preparation of the wheat embryo extract useful for the cell-free reactions, by which 5 ml of a high-activity extract is obtained in 4–5 d. We also describe the methods for small- and large-scale protein synthesis by hands-down operations with the use of mRNAs prepared by transcription of PCR products and pEU plasmids harboring the target cDNAs, which need 2–4 d excepting the time required for plasmid preparation.

INTRODUCTION

With much information on the genome and cDNA sequences of many different organisms, we can now obtain and deduce a lot of information about the gene products and their interactions with the aid of bioinformatics, genetics and cell biology. However, such pieces of information are in many cases a result of presumption, or an extrapolation from known facts. To understand specific biochemical phenomena at the molecular level, *in vitro* analyses of biochemically characterized samples are strictly required. Conventionally, biochemists had to purify their samples, i.e., proteins and other biomolecules, from living organisms. The recombinant expression technologies that emerged in the late twentieth century helped them greatly. However, although there is a lot of information and a lot of potential targets to be analyzed, the preexisting technologies do not meet the need to prepare sufficient sized samples of many different proteins.

Cell-free protein synthesis was developed in the middle of the last century. It entered the limelight as a method for the preparation of proteins when the continuous-flow cell-free method was developed by Spirin *et al.*[1] in 1988, in which fresh substrates were supplied into and byproducts were removed from the reaction chamber continuously during the reaction with the extract from *E. coli* or wheat embryos. Our group found that the instability that had been observed for the translation with wheat extracts prepared by conventional methods arose from intrinsic factors that catalytically inhibited translation[2], and developed a method to eliminate the catalysts. Here, we describe the method for preparation of the extract as well as the basic techniques for parallel preparation of many different proteins for functional analyses and those for a large-scale preparation that may be applicable to structural analyses and antigen preparation. These technologies are based essentially on the following three elemental technologies: a method for eliminating the contaminants from the endosperm in the wheat embryo extract, which keeps up the inherent robustness of the natural translation apparatus[2], the PCR-based high-throughput method for preparation of DNA templates (the 'split-primer PCR' method)[3] and a reaction format that fit to highly parallel operation (the 'bilayer' method)[4]. A more detailed history of the development of the wheat cell-free system has been reviewed elsewhere[5,6]. The most prominent advantage of the wheat cell-free method, as recognized by our group through the collaborations with many other groups, is the high quality of the produced proteins, particularly when cytosolic proteins from eukaryotic origins are produced[7] (see below in the 'Applications of the method' section).

The cell-free protein synthesis system from *E. coli* is also capable of both highly parallel protein production and mass production. The wheat system has an advantage over the *E. coli* system in the probability of producing human proteins in soluble forms as clearly demonstrated[7]. This is probably due to the eukaryotic nature of the wheat system. In addition, machines for production of proteins are commercially available for the wheat system, as below. On the other hand, the productivity per reaction time may be higher in the *E. coli* system than in the wheat system. In addition, the method for preparation of the cell extract at the laboratory level is less laborious in the *E. coli* system. As a result, the cost of the extract is lower in the *E. coli* system. Thus, if one wishes to produce polypeptides in insoluble forms, the *E. coli* system has a clear advantage both in the cost and the productivity. The *E. coli* system also has an advantage in the production of bacterial soluble proteins that can fold properly in bacterial cells, as the cost of the extract is lower. Although we do not have clear statistical data, it seems that the codon usage bias in the open reading frame (ORF) sequence to be translated affects the productivity much less severely in the wheat system[8].

The wheat cell-free protein synthesis system has been commercialized by CellFree Sciences (CFS). The products of CFS, including the wheat embryo extract (cat. nos. CFS-TRI-1240/1240H/1240G), have highly controlled qualities, and they come with detailed protocols when purchased. Thus, we start with a method for preparation of the extract, for those who are hesitant to purchase the extract. As the extract is stable at −80 °C for years, it is less convenient to prepare small amounts of the extract at a time. In addition, we have already described the small-scale method several times elsewhere[9,10]. Thus, we show here a large-scale method[11]. The extract prepared by this protocol fits to the CFS protocols. We then describe the 'bilayer' methods for small-scale high-throughput parallel protein synthesis in a microtiter plate and those for larger scale preparation, which are essentially the same as that in the CFS protocols and are most convenient at present. A diagram showing the procedure is in **Figure 1**.

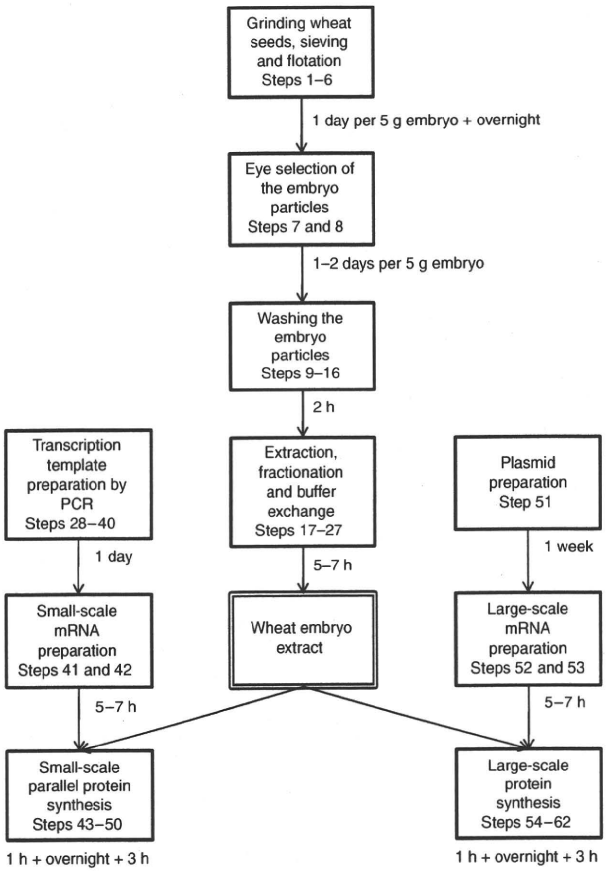

Figure 1 | Summary of steps involved in the procedure.

Experimental design

Preparation of unwashed embryo particles. The primary (unwashed) embryo particles are prepared by crushing wheat seeds with a mill followed by sieving and selection. Typically, 1 kg of wheat seeds gives around 1 g of crude embryo particles.

The most important step in the preparation of a good extract is to obtain an ensemble of good embryo particles that attach minimal amounts of endosperm to be washed out in the next step. This is possible at present only by selecting the particles apparent to human eye. This eye selection is the toughest step for laboratory workers. Thus, we use conventional methods to select the particles crudely by flotation before selection by eye. However, this raises the problem of organic-solvent waste containing carbon tetrachloride. Therefore, we now use the extract supplied by CFS for ordinary experiments. Nevertheless we describe here the method including the flotation selection step, expecting that the researchers who can use carbon tetrachloride in the laboratory may be able to perform the experiments themselves. The flotation steps may be omitted if more time and effort can be invested in the eye selection. We have not tested if other liquids could be used for the purpose, such as pure methylene chloride that has a density close to the one used in the present procedure and high-density aqueous solutions of polymers and/or salts.

Preparation of the extract. The embryo particles should be washed extensively before being crushed. This will eliminate translation inhibitors that come from endosperm. Conventionally, we crushed up to several grams of the washed embryo particles with mortar and pestle under liquid nitrogen in a cold room[2,9,10]. Here, we describe a patented method using a food processing mill/mixer, which has facilitated a larger-scale preparation of the extract with higher activities and has eliminated the risk of choking in the cold room associated with the use of liquid nitrogen[11]. While we used a popular food processor, a conventional Waring Blender can also be used. Although we usually start with 60 g of unwashed embryo particles, the amount of the starting material can be reduced down to several grams. The smallest amount that could be crushed properly is dependent on the size of the blender cup. A machine that can grind green tea may be useful for smaller-scale experiments, although we have not tested any. Once a large amount of the extract is prepared, it can be stored at −80 °C for at least a year.

Conventionally, we prepared the extract in the extraction buffer (EB, see below). However, we found that the buffered substrate mixture as below (BSS) is useful and more convenient than the EB, because preparation of the translation reaction mixture can be simpler, which is important for high-throughput applications.

The translational activator sequences. The mRNA molecules to be translated in the wheat cell-free system should have a translational enhancer sequence in the 5′-untranslated region (UTR)[3,12]. We have observed that the introduction of a cap structure at the 5′ end of mRNA molecules by a standard transcription method does not work well unless the mRNA concentration to be used for translation is optimized for each preparation. The 3′-UTR of the mRNA molecules should be at least as long as 500 nt, while no sequence preferences have been observed. Thus, 3′-UTR can contain the sequence from the vector in which the ORF to be translated is subcloned.

Template preparation by PCR. We describe a method for preparation of transcription-ready PCR fragments with a 5′-enhancer sequence and a long 3′ sequence[3], by which many different cDNA clones could be amplified in parallel. The PCR method comprises two steps. In the first PCR, a 5′ gene-specific primer and the AODA2306 primer (see **Table 1** and **Fig. 2a,b**) are used. The gene-specific primer should be designed for each gene to be expressed so that it hybridizes with the first 20 bases of the ORF to be amplified as in **Table 1**. It should introduce a short leader sequence. The

TABLE 1 | Oligodeoxyribonucleotides.

Name	Sequence	Convenient stock concentration (μM)
AODA2303	5′-GTCAGACCCCGTAGAAAAGA-3′	1
AODA2306	5′-AGCGTCAGACCCCGTAGAAA-3′	0.1
deSP6E01	5′-GGTGACACTATAGAACTCACCTAT CTCCCCAACACCTAATAACATTCAAT CACTCTTTCCACTAACCACCTATCTAC ATCACCACCCACCACCACCAATG-3′	0.1
SPu	5′-GCGTAGCATTTAGGTGACACT-3′	1
Gene-specific primer	5′-CCACCCACCACCACCAATGNNN NNNNNNNNNNNN-3′	0.1

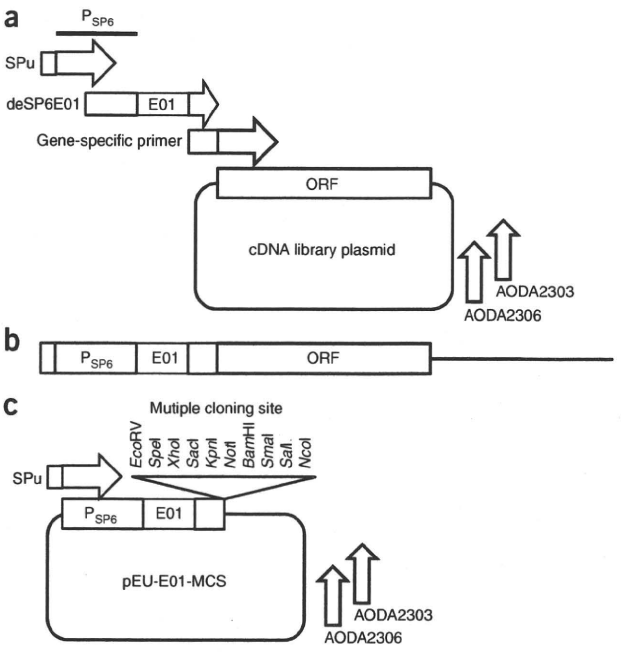

Figure 2 | Schematic representations of DNA molecules. (**a**) Positions of the primers used for the two PCR amplifications are indicated with a schematic representation of a typical cDNA library plasmid clone. The two downstream primers hybridize near the plasmid origin, and thus the library vector should have the same sequence, and the ORF of the library clone should be inserted in this direction. The gene-specific primer and AODA2306 are used for the first PCR, and the other three primers are used for the second PCR. (**b**) An illustration of the transcription-ready template DNA that should be generated after the second PCR. (**c**) An illustration of pEU-E01-MCS, which is provided in the CFS kits and is useful for cloning of the cDNA sequence to be expressed in the wheat cell-free translation system.

AODA2306 primer is designed to hybridize within the replication origin region of the pUC plasmids, which is present in many cDNA library vectors. In the second PCR, AODA2303, deSP6E01 and SPu are used as primers. AODA2303 hybridizes three bases closer to the ORF than the position for AODA2306. deSP6E01 is a long oligonucleotide containing a partial SP6 promoter sequence lacking the 5′ five bases, the E01 sequence, and the leader sequence that is also in the 5′ region of the gene-specific primer. This primer is used in a lower concentration. The E01 5′ enhancer sequence used here can be substituted with the E02 sequence[12] or by the Ω sequence from tobacco mosaic virus. SPu contains the 5′ 14 bases of the SP6 promoter sequence in the 3′ part (the 3′ 9 bases overlaps with the 5′ region of deSP6E01). It is important to split the promoter sequence so that no primer has a complete promoter sequence because this dramatically reduces the possibility of generating nonspecific amplification of transcribable sequences. This 'split-primer' method is not required if the cDNA clones are inserted into pEU as described below.

Small-scale parallel protein synthesis. The PCR products can be transcribed into mRNA by a simple enzymatic reaction. The transcription products can be transferred directly into the translation mixtures. The bilayer method described here is suitable for parallel translation of many different mRNA samples, as it can be performed in microtiter plate wells and is much more efficient than a simple batch reaction. The reaction mixture containing the extract is slightly heavier than the substrate solution, and these two solutions can form a bilayer. Translation starts within a small space with concentrated initiation factors and ribosomes, forming polysomes. As the reaction proceeds, the byproducts are gradually diluted into the upper substrate solution, and the fresh substrates gradually diffuse into the reaction site. Thus, it is very important not to mix the two layers. Robots performing this procedure by parallel operations are available from CFS.

Conventionally, we adjusted the concentrations of the ingredients in the starting reaction mixture that should be layered under the substrate mixture to those of the components in the BSS substrate mixture. However, we have found that this is not necessary, probably because low-molecular-weight compounds will diffuse rapidly into the reaction mixture from the substrate mixture. In addition, it has been found to be unnecessary to remove the white insoluble material generated during the transcription reaction. The protocol shown here is thus quite simple: just mixing three solutions, including the extract, the transcription product and the creatine kinase solution. This simplicity has made this protocol more useful for high-throughput parallel production of many different proteins.

The concentrations of magnesium and potassium ions can affect the translation efficiency, whereas the transcription buffer contains a higher concentration of magnesium ions and no potassium ions, which may cause inefficient translation. However, we have observed no problem in the efficiency of translation. This may be because small ions can exchange rapidly between the reaction and substrate mixtures. It is also possible that the magnesium pyrophosphate precipitate may be serving as a buffer of magnesium concentration.

The pEU expression vector. The pEU vector contains an SP6 promoter, a translational enhancer and a multiple cloning site (**Fig. 2c**). This vector is suitable for large-scale expression of the subcloned ORF in the wheat cell-free system. Control pEU plasmids, such as that harboring the GFP cDNA, are available on request. Various pEU plasmids with inserted tags are also available. We are also ready to distribute a Gateway destination vector of pEU on request: various entry vectors for the human cDNA clones are also available from the National Institute of Technology and Evaluation, Japan[7].

Large-scale protein synthesis. We describe here the method for the bilayer mode large-scale protein synthesis with an mRNA solution prepared by direct transcription of the pEU plasmid template harboring the ORF sequence to be translated. For large-scale synthesis, more productive methods are available (see below). However, the present method is the simplest to be performed and thus fits with automation. The transcription template can also be prepared by PCR amplification of the plasmid sequence with the SPu and AODA2303 primers. We recommend the direct transcription method here just because the method is simpler than that including a PCR step.

Control reactions that should be added. pEU-E01-DHFR, which is available from CFS and from our laboratory, can be used for a positive control reaction for large-scale protein synthesis. For the small-scale experiment, an aliquot from the large-scale transcription product from pEU-E01-DHFR can be used. When only one sample is tested, the sample with no mRNA (water should be

added instead of the mRNA solution) may be used as a negative control, which will help to identify the band of the synthesized protein on the electrophoresis gel among the other bands arising from the components of the extract. If plural different mRNA samples are translated, we usually perform no negative control reaction because each band can be identified by comparison with the other lanes.

Applications of the method

Examples of expressed proteins. We have already tested many different proteins for the productivity in the wheat cell-free system. An encompassing list of successful proteins would be so large that we could not show here. Lists of the successful examples at the time point of 2006 are elsewhere[5]. In such examples, the details of the methods for translation were different from the exact one presented here: as far as we know, success in production of a protein does not depend on the details and the reaction modes described below. Recently, 13,361 human cDNA clones were tested if they were translated in the wheat cell-free system by a bilayer protocol. It was found that 12,996 produced a detectable amount of the polypeptide and that 12,682 were detectable in the soluble fraction, of which 3,040 contain at least one predicted transmembrane domain[7]. Therefore, we believe that most cDNA sequences can be translated into the polypeptide sequences, unless the polypeptide interferes severely with the translation machinery. We have observed that many of the eukaryotic protein kinases can be produced in the active forms in the wheat translation system, while this group of proteins is recognized to be generally difficult to be produced in bacterial systems[5]. In particular, human calcium/calmodulin-dependent protein kinase II delta produced by this method readily phosphorylated novel natural substrates within a HeLa cell extract[13]. We have also produced plant RNA ligase, production of which has been reported to be difficult using bacterial expression systems[14]. It has been suggested that the wheat system has an advantage over bacterial systems in proper folding of multidomain proteins from eukaryotic origins, in particular those with a domain with a high β-strand contents[15]. This may be a result of coevolution of protein sequences and the protein synthesis apparatus, which might have been the origin of various protein functions in eukaryotic cells that confer the dazzling complexity of the eukaryotic organisms. On the other hand, some prokaryote-specific proteins might be produced in an inactive form in the wheat system: we have observed that a bacterial protein with a deep trefoil knot structure is not produced in its fully active form[16]. cDNAs with highly biased codon usages are also difficult to be expressed in bacterial systems. We have already expressed many *Plasmodium* cDNAs that have very high A/T contents successfully[8]. Proteases are generally difficult to be produced *in vitro* because of their activity. However, the wheat cell-free system sustains the translation activity even at 4 °C, and we have already confirmed that some proteases can be produced successfully (our unpublished data). Formation of proper quaternary structures has been observed for several proteins. The crystalline particles of polyhedrin were observed when its mRNA was translated[17]. A heterodimer enzyme was found to fold properly only when synthesized simultaneously in a reaction mixture containing the mRNA molecules for both subunits[18], whereas another heterodimer enzyme had its activity even when each subunit was synthesized separately and mixed with each other after purification[19]. There are only a limited number of examples of disulfide containing proteins and membrane proteins that were expressed efficiently as below. It is very difficult to introduce sugar modifications onto proteins, in part because the endoplasmic reticulum is absent from the extract and, in part, because the extract contains enzymes that degrade sugars.

The PCR method, fusion proteins and high-throughput production. The PCR method presented here can be modified in many ways. In fact, the templates for the human proteins above were amplified from *in vitro* recombinants produced in the Invitrogen Gateway system without transformation[7]. The templates for fusion proteins can be produced easily by PCR, and more than 500 different fusion proteins have been tested for their solubility and activities virtually by one person[15]. This was possible because proteins produced in the wheat system were generally quite stable. The stability is due to the lack of the 26*S* proteasome-dependent protein degradation activity[20]. It was also possible to manually produce many different proteins with different N-terminal sequences for a systematic analysis of the N-end rule in the wheat cell-free system[21]. N-terminal small tags, such as 6× His tag, can be fused to any protein by simply changing one primer used in the present PCR protocol. Larger tags such as glutathione-*S*-transferase can also be fused by including a small amount of the DNA fragment encoding the tag. These fusion technologies were successfully used for a high-throughput parallel assay of many different transcription factors encoded in cDNA library clones[22]. This type of rapid parallel assay and screening of many different proteins, we believe, will become very important for the post-genomic researches. A basic technology for construction of a protein chip with the proteins fused to a DNA-binding protein has also been developed[23]. The use of PCR for rapid template preparation was also shown to have a potential to accelerate protein engineering[24]. Most of these high-throughput applications have been performed according to older and more complicated protocols than the one that we show here. The present small-scale protein synthesis protocol can be applied to the parallel production of hundreds of different proteins just by performing it in parallel, using a multichannel pipette or the machine mentioned below.

Reaction modes for the cell-free translation. There are several reaction formats for translation. Although we present here the method for translation in the bilayer mode, the other formats are also possible with the extract prepared by the present procedure. Different reaction formats have been summarized elsewhere[9,10]. The batch mode translation, in which the reaction is performed in a homogeneous solution, is useful for testing the activity of the extract and mRNA preparations. For the batch mode synthesis, a fourfold concentrated solution of the substrates (4× BSS, see below) is useful for preparation of the starting mixture in 1× BSS with creatine kinase. In this case, the test can be more sensitive and quantitative if a radiolabeled amino acid is included in the reactions. The dialysis mode translation, in which the reaction is performed within a dialysis bag or a dialysis cartridge with continuous dialysis against the substrate solution, is generally more efficient than the bilayer method. The discontinuous batch (or 'repeat-batch') method[10], in which the buffer/substrate is forcibly exchanged during the translation reaction repeatedly, is very productive, although it needs a machine to be performed. A machine that performs the discontinuous batch mode translation reaction

for gram-scale synthesis is available from CFS, and the protocols for the machine are available in the CFS website. Machines for the bilayer mode parallel translation reactions for high-throughput applications are also available from CFS.

Amino acid labeling for protein structural analyses. The wheat translation system has also been applied to structural biology. This utilizes the high productivity and ease of amino-acid-specific labeling. NMR heteronuclear single quantum coherence (HSQC) spectra could be obtained by measuring the translation product with uniformly labeled amino acids almost without purification: only after a buffer exchange and removal of the precipitant[25]. This is very useful for high-throughput assessing the 'foldedness' of the structural biology samples[26]. The wheat cell-free system has already been modified to fit to a large-scale screening of proteins that are suitable for NMR-based structure determination[26,27]. Amino-acid-specific isotope labeling is also possible with only two transaminase inhibitors added to the translation reaction that prevent scrambling of the isotope caused by metabolic reactions[28–30]. This method may be useful also for the labeling with the stereo-array isotope labeling (SAIL) amino acids, which is expected to accelerate NMR structural analyses[31]. For these applications, the dialysis method may be more useful than the present bilayer method. Selenomethionine substitution of methionine residues in proteins is also easy with the wheat cell-free system, and an X-ray structure of a restriction enzyme has been determined[32].

Modification of the extract. The extract is resistant to many chromatography resins and ultrafiltration membranes. Therefore, it is possible to pretreat the extract with glutathione sepharose or with a metal-chelating resin in order to remove the binders arising from the wheat embryos. Such extracts are available from CFS. It is also possible to freeze-dry the extract without a severe loss of activity, and the freeze-dried extract is stable at least 3 years at −20 °C. We believe that the protein synthesis machinery within embryo cells in natural situations is preserved in a dehydrated state in the winter before imbibition in the spring. We are developing educational experiment kits including a freeze-dried extract, which can be stored stably even in a household freezer that most high schools may be equipped with. It may help the students to feel and understand the relationships between genetic information and protein function and between life and matter.

Other options. Many other applications are possible by modifying the materials added to the reaction. A cofactor-binding protein has been synthesized in the presence and absence of the cofactor, and it was found that both holo-forms and apo-forms could be produced, which was useful for the study of the architecture of the enzyme[10,33]. Disulfide bond formation may be inefficient in the wheat cell-free system because of the presence of DL-dithiothreitol (DTT) in the reaction mixture. By omitting DTT from the substrate mixture, disulfide bonds in some proteins may be formed, although the efficiency of protein synthesis are limited[7,34]. Some membrane proteins have been synthesized in their active forms in the presence of liposomes or some detergents[35–37]. It was also possible to select some functional sequences from a random pool of mRNA molecules, through which the E01 sequence used in the present protocols has been obtained[12]. The lack of the proteasome activity[20] may help us to reconstitute intracellular multicomponent molecular systems, such as protein degradation systems, without purification of each component. We believe that the wheat translation system may be useful also for synthetic biology purposes.

MATERIALS

REAGENTS

- Unsterilized wheat seeds (strain 'Chihoku': any strain may be used): dried after harvesting, unbaked and containing no pesticides or insecticides (as one may be exposed to the drugs when crushing the seeds)
- Nonidet P-40 (NP-40; Nacalai Tesque, cat. no. 23640-94) ! **CAUTION** Harmful (wear gloves).
- Cyclohexane (Wako Pure Chemicals, cat. no. 034-05001) ! **CAUTION** Highly flammable, harmful and dangerous for the environment (wear gloves and handle the reagent in a fume hood).
- Carbon tetrachloride (Wako Pure Chemicals, cat. no. 039-01271) ! **CAUTION** Toxic and dangerous for the environment. Use of this reagent is tightly regulated in Japan. Wear gloves and handle the reagent in a fume hood. Confirm and obey local regulations associated with the use and disposal of the reagent.
- 2-[4-(2-Hydroxyethyl)-1-piperazinyl]ethanesulfonic acid (HEPES; Nacalai Tesque, cat. no. 17514-15) ! **CAUTION** Irritant.
- Potassium hydroxide (Nacalai Tesque, cat. no. 28616-45) ! **CAUTION** Corrosive (wear gloves and protecting glasses).
- Potassium acetate (Nacalai Tesque, cat. no. 28405-05)
- Magnesium acetate tetrahydrate (Nacalai Tesque, cat. no. 20821-85)
- Calcium chloride (Nacalai Tesque, cat. no. 06729-55)
- DL-Dithiothreitol (DTT; Wako Pure Chemicals, cat. no. 049-08972)
- Standard 20 L-amino acids (Wako Pure Chemicals or Nacalai Tesque)
- Milli-Q water (freshly prepared with a Millipore system, Millipore)
- Elix water (produced with a Millipore system, Millipore)
- Sodium acetate (Nacalai Tesque, cat. no. 31119-65)
- Acetic acid (Nacalai Tesque, cat. no. 00212-56) ! **CAUTION** Flammable (handle in a fume hood).
- Ethanol (Nacalai Tesque, cat. no. 14713-95) ! **CAUTION** Highly flammable (handle in a fume hood).
- Sephadex G-25 Fine (GE Healthcare, cat. no. 17-0032-01)
- TaKaRa *Ex* Taq (Takara Bio, cat. no. RR001A)
- Plasmid preparation kit (QIAGEN Plasmid Midi Kit, QIAGEN, cat. no. 12143)
- ATP, disodium salt (Sigma, cat. no. A3377)
- GTP, sodium salt (Sigma, cat. no. G8877)
- CTP, disodium salt (Sigma, cat. no. C1506)
- UTP, trisodium salt (Sigma, cat. no. U6625)
- Spermidine (Rnase-free, Sigma, cat. no. S0266) ! **CAUTION** Corrosive (wear gloves).
- Creatine phosphate (Wako Pure Chemicals, cat. no. 030-04584, or Roche, cat. no. 621722)
- Creatine kinase (Roche, cat. no. 127566)
- SP6 RNA polymerase (HC) (80 U μl^{-1}, Promega, cat. no. P4084)
- RNasin Ribonuclease Inhibitor (20–40 U μl^{-1}, Promega, cat. no. N2511)
- Oligodeoxyribonucleotides listed in **Table 1** (Invitrogen)
- Liquid nitrogen ! **CAUTION** Wear nonpermissible gloves; obey local regulations.

EQUIPMENT

- Rotor Speed Mill PULVERISETTE 14 (Fritsch)
- Sieve shaker (A-3 PRO, Fritsch) with 710-, 850- and 1,000-μm mesh sieves (The Iida Testing Sieves, Iida Manufacturing)
- Sonicator (W-113 Ultrasonic Cleaner, Honda Electronics)
- Fume hood
- Blender (KC-4811W Mill & Mixer, Twinbird)
- Amicon Ultra-15 (10 kDa, Millipore, cat. no. UFC9 010 08)
- Toothpicks
- Mesh skimmer
- Kimwipe sheets
- Kim Towels
- Corner trash bags ('Gomipon', Kokubo): alternatively, nylon stockings may be useful

- Hitachi CR21G centrifuge with an R10A3 rotor (Hitachi, cat. no. 904308D0) with 500-ml centrifuge bottles (cat. no. 330437A)
- TOMY GRX-220 centrifuge with a TA-24BH rotor (TOMY), with 50-ml round-bottom centrifuge tubes (cat. no. 3177-9500; capped with DS3119-0029 centrifuge tube closures)
- 50-ml injection syringe (Terumo, cat. no. SS-50ESZ)
- Cotton wool
- Aluminum foil
- Air incubator (MIR-153, SANYO)
- UV spectrophotometer (Beckman DU600, Beckman)
- Submarine-type and slab gel electrophoresis systems for agarose and SDS-polyacrylamide gel electrophoresis, respectively
- UV light and camera (Toyobo)
- PCR machine (PCR Thermal Cycler MP, Takara Bio)
- 96-well microtiter plate (Techno Plastic Products AG, cat. no. 92096)
- 6-well plate (Techno Plastic Products AG, cat. no. 92006)
- pH meter
- Autoclave

REAGENT SETUP

Cyclohexane/carbon tetrachloride mixture Mix 2.4 volume of carbon tetrachloride with one volume of cyclohexane. Handle and store it in a fume hood at room temperature (20–25 °C). The mixture can be reused several times.

0.5% (vol/vol) NP-40 solution Dissolve NP-40 in Milli-Q water. Store it at room temperature (stable for years).

3 mM amino acid mixture Dissolve all of the 20 standard amino acids into Milli-Q water. For storage, seal the container tightly to avoid air oxidation and store it frozen at −20 °C (stable for at least a year).

2× EB Mix 80 mM HEPES-KOH (pH 7.6), 200 mM potassium acetate, 10 mM magnesium acetate, 4 mM calcium chloride, 0.6 mM amino acids and 8 mM DTT freshly at 4 °C. ▲ CRITICAL Use it in a few days.

5× Transcription buffer (TB) Mix 400 mM HEPES-KOH (pH 7.8), 80 mM magnesium acetate, 10 mM Spermidine and 50 mM DTT. Store it in aliquots at −20 °C (stable for at least a year).

3 M Sodium acetate Add 3 M acetic acid to a 3 M sodium acetate solution and adjust to pH 5.2. Sterilize the solution by autoclaving or by filtration. Store it at room temperature (stable at least a year).

70% (vol/vol) ethanol Mix 35 ml of ethanol and 15 ml of Milli-Q water. Store at −20 °C (stable at least a year).

100 mM ATP, CTP, GTP and UTP Dissolve the powder of the salt of the nucleotide in water and adjust pH of the solution between 7 and 8.5. Measure the absorbance at 260 nm and adjust the concentration to 100 mM by adding water according to the molecular extinction coefficient of 15.4, 9.0, 11.4 and 9.9×10^3 cm^{-1} M^{-1} for ATP, CTP, GTP and UTP, respectively. Store each solution frozen at −80 °C (stable for a year).

NTP solution Mix equal volume of 100 mM ATP, CTP, GTP and UTP. Store it frozen at −80 °C (stable for a year).

20 mg ml^{-1} Creatine kinase Dissolve the powder in water and store it in aliquots at −80 °C (stable at least a year).

4× Buffered substrate solution (BSS) 120 mM HEPES-KOH (pH 7.6), 400 mM potassium acetate, 10.8 mM magnesium acetate, 1.6 mM spermidine, 10 mM DTT, 1.2 mM amino acids, 4.8 mM ATP, 1 mM GTP and 64 mM creatine phosphate. Store it in aliquots at −20 °C (stable for 2 months).

1× BSS Dilute 4× BSS with Milli-Q water. Prepare just before use; can be stored for a few days at −20 °C.

EQUIPMENT SETUP

Rotor speed mill Set the rotor speed to 7,000 r.p.m. The mill and the sieve shaker will produce a lot of fine powder of flour, which floats around in the air and contains inhibitors of protein synthesis. Thus, these equipments may be better kept away or spatially isolated from the biochemical laboratory.

A-3 PRO shaker Set the amplitude to 2.0 mm, sieving time to 2 min and interval to 1 s. This may also be isolated from the biochemistry laboratory.

The blender Use the larger cup (200 ml mixer cup) for 60 g embryo. The smaller (70 ml) cup may be useful for the preparation from smaller amounts (less than around 20 g) of the purified embryo particles.

Sonicator Add ice to the water in the top bucket. Set the frequency to 45 kHz.

PCR thermal cycler Program 1: 94 °C for 4 min; 30 cycles of 98 °C for 10 s, 55 °C for 1 min and 72 °C for 1 min per 1-kb amplified sequence; and 72 °C for 5 min. Program 2: 94 °C for 4 min; 5 cycles of 98 °C for 10 s, 55 °C for 1 min and 72 °C for 1 min per 1-kb amplified sequence; 35 cycles of 98 °C for 10 s, 60 °C for 40 s and 72 °C for 1 min per 1-kb amplified sequence; and 72 °C for 7 min.

PROCEDURE

Preparation of unwashed embryo particles ● TIMING 2–3 d per 5 g embryo particles from 5 to 6 kg seeds

1| Grind the wheat seeds in the mill at the rate of 100 g per min. Repeat this four times.

! CAUTION Wear protectors if needed, because fine powder will drift around in the air.

2| Shake the sample in the sieve shaker.

3| Collect the particles on the 850- and 710-μm sieves in a dish.

4| Let the sample fall onto another dish from around a 50-cm height repeatedly to remove seed-coat fragments.

5| Pour the particles into a beaker containing around 1 l of cyclohexane/carbon tetrachloride mixture in the fume hood and stir the mixture thoroughly. Do not leave the embryo particles in the solvent too long.

6| Collect the floating particles with a mesh skimmer as fast as possible after the particles are separated, and put them on Kimwipe sheets in the fume hood to remove the solvent overnight.

■ PAUSE POINT The embryo particles can be stored at 4 °C for several years.

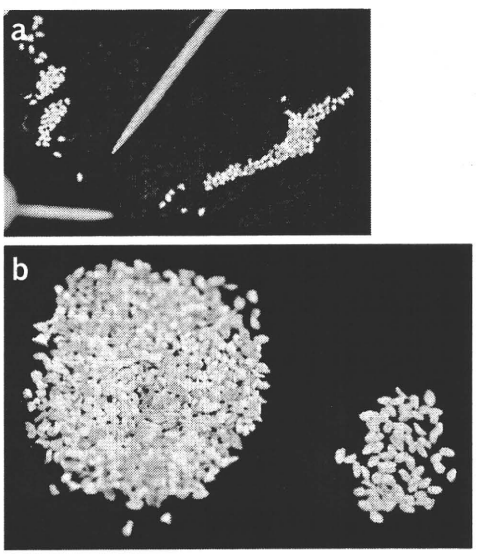

Figure 3 | Selection of good embryo particles by eye. (**a**) Selecting good particles using a toothpick. (**b**) Good particles (left) and bad particles (right).

7| Spread the particles on a clean paper or plastic sheet on a desk. Select only those particles with yellow color with a minimum amount of white matter attached to them using a toothpick, carefully investigating each particle by eyes: remove brownish particles and the particles with much white matter coming from endosperm (**Fig. 3**).
▲ **CRITICAL STEP** The white matter contains the catalytic inhibitors of protein synthesis.

8| Store the selected particles at 4 °C until use.
■ **PAUSE POINT** The embryo particles can be stored at 4 °C for several years.

Preparation of the extract ● TIMING **1 d**

9| Put 60 g of embryos in a corner trash bag. A smaller amount may also be washed successfully, although we have only a little experience. Wash the particles in a stream of 5-l cold Elix water.

10| Dip the bag in cold Elix water (4 °C, typically 700 ml) and knead it gently. Do not knead it too much.

11| Change the water and repeat Step 10 several times more until no white matter disperses out through the bag.

12| Change the water to 500 ml of 0.5% NP-40 solution (4 °C) and sonicate the sample for 5 min with gentle stirring.

13| Wash in an Elix water stream (typically 3 liters, not chilled) until no bubbles can be seen, and sonicate twice in cold Elix water.

14| Wash the particles five times more in a beaker with 800 ml each of cold Milli-Q water.

15| Take out the embryo particles and wrap them in Kimwipe sheets, which are further wrapped with a sheet of Kim Towel, in order to remove water.

16| Repeat this wiping a few times until no more water can be removed.

17| Put the washed embryo particles from 60 g of the starting unwashed embryos (around 120 g) in the larger (mixer) cup of the blender and add 90–120 ml of 2× EB (4 °C). We have confirmed that 10 g of the washed embryo particles could also be processed successfully with 10 ml of 2× EB in the smaller cup.

18| Run the blender for 30 s three times.

19| Centrifuge the sample at 30,000*g* at 4 °C for 30 min in a TA-24BH rotor with the GRX-220 centrifuge (**Fig. 4**). Collect the supernatant, i.e., the middle layer between the fatty material and the precipitate.

20| Centrifuge the sample again at 30,000*g* at 4 °C for 15 min in a TA-24BH rotor with the GRX-220 centrifuge and collect the supernatant in a tube.

21| Pass the sample through a G-25 column pre-equilibrated with 1× EB. A 40-ml column may be prepared in a 50-ml injection syringe with cotton wool at the bottom, which can be hung at the rim of a 500-ml centrifuge bottle in it, loaded with maximum of 20 ml of the sample, capped with aluminum foil and centrifuged at 750*g* for 5 min at 4 °C in a R10A3 rotor.

22| Pass the sample through a G-25 column pre-equilibrated with 1× BSS.

23| Measure the absorbance of the extract at 260 nm in a 1-cm path length cuvette (a several hundred-fold dilution will be needed), which may be more than 150. If the absorbance is, e.g., 160, then the concentration of the extract is 160 AU ml^{-1}, where '1 AU' is the amount of the extract that gives the absorbance of 1 at 260 nm in a 1-cm

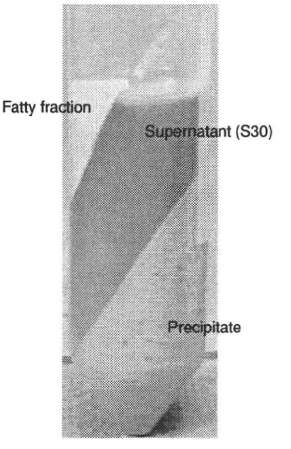

Figure 4 | An example of the sample after the first 30,000*g* centrifugation. The sample in Step 19 may be separated as in the figure (in which a conical tube is used).

path if dissolved in a 1-ml solution. The manuals from CFS use 'OD' instead of 'AU.'
? TROUBLESHOOTING

24| Concentrate the extract to around 300 AU ml^{-1} by ultrafiltration with 10 kDa Amicon Ultra-15 cartridges. Eight cartridges can be centrifuged at once in the TA-24BH rotor.

25| Pass the sample through a G-25 column pre-equilibrated with 1× BSS again.

26| Measure the absorbance at 260 nm of the extract and adjust the concentration to 240 AU ml^{-1}.
? TROUBLESHOOTING

27| Aliquot the sample and freeze each tube quickly in liquid nitrogen. Store them at −80 °C. Do not store the extract at −20 °C.
■ PAUSE POINT The extract is stable for at least a few years at −80 °C.

Template DNA preparation for small-scale parallel protein synthesis ● TIMING **1 d**
28| Mix 0.5 ng of the plasmid containing the target cDNA sequence in a PCR tube on ice with 10 nM of the target-specific primer, 10 nM of the AODA2306 primer, 200 μM each of dNTP, the buffer supplied by the supplier and 0.0125 U μl^{-1} of *Ex* Taq DNA polymerase in a 20-μl reaction mixture (**Fig. 2**). When many different reactions are performed in parallel, mix the materials other than the plasmid and the target-specific primer in one tube and dispense this mixture to the plasmid/target-specific primer solution. Set the sample(s) in PCR Thermocycler and run it with Program 1.

29| Check the amplified DNA by agarose gel electrophoresis.
■ PAUSE POINT PCR products may be stable at −20 °C for years.
? TROUBLESHOOTING

30| Mix 5 μl of the first PCR product (without any purification) in a 200-μl PCR tube with 100 nM each of the SPu and AODA2303 primers, 1 nM of the deSP6E01 primer, 200 μM each of dNTP, the buffer supplied by the supplier and 0.0125 U μl^{-1} of *Ex* Taq DNA polymerase in a 50-μl reaction mixture (**Fig. 2**). For parallel preparation, mix everything other than the first PCR product in one tube and dispense it into each PCR tube before putting in the first PCR product. Put the sample(s) in PCR Thermocycler and run it with Program 2.

31| Add 5 μl of 3 M sodium acetate (pH 5.2) and 140 μl of ethanol to each of the second PCR solutions. Mix the samples well. Incubate them at −20 °C for 10 min.

32| Centrifuge the samples at 15,000*g* for 15 min at 4 °C in a standard microcentrifuge.

33| Remove the supernatant and add 300 μl of chilled 70% ethanol.

34| Centrifuge the samples at 15,000*g* for 5 min at 4 °C.

35| Remove the supernatant carefully and thoroughly and dry the samples with the tube lids open covered with Saran Wrap.

36| Add 10 μl of Milli-Q water to each sample and dissolve the pellets well.

37| Analyze 1 μl of the samples by agarose gel electrophoresis. Estimate the concentration of the DNA by comparing with the bands of the molecular weight marker run in the same gel. Adjust the concentration of each sample around 0.25 $\mu g\ \mu l^{-1}$.
■ PAUSE POINT PCR products are stable at −20 °C for years.
? TROUBLESHOOTING

mRNA preparation for small-scale parallel protein synthesis ● TIMING **5–7 h**
38| Prepare a solution containing 6 μl of 5× TB, 3 μl of 25 mM NTP, 48 U of RNase inhibitor and 48 U of SP6 RNA polymerase per 16 μl using Milli-Q water. This gives the 1.5× final buffer concentration. Dispense 16 μl of this solution in each well of a microtiter plate. Add 4 μl of the second PCR solution and incubate the plate at 37 °C for 4–6 h. White insoluble material will be generated during transcription.

39| Analyze the product (1 μl) in a 1% (wt/vol) agarose gel stained with ethidium bromide.
■ PAUSE POINT The sample can be stored at −80 °C for weeks. Transportation with dry ice is not recommended.
? TROUBLESHOOTING